National Technical University of Athens
School of Mechanical Engineering
Fluids Section
Parallel CFD & Optimization Unit

Multidisciplinary Analysis and Optimization under Uncertainty. Application to a Fire Monitoring Satellite

Diploma Thesis

Vasileiadis Orfeas

Advisors:
Kyriakos C. Giannakoglou, Professor NTUA
Dr. V. Asouti, Adjunct Lecturer NTUA

Athens, 2026

National Technical University of Athens
School of Mechanical Engineering
Fluids Section
Parallel CFD & Optimization Unit

Multidisciplinary Analysis and Optimization Under Uncertainties. Application to a Fire Monitoring Satellite

Diploma Thesis

Vasileiadis Orfeas

Advisors:
Kyriakos C. Giannakoglou, Professor NTUA
Dr. V. Asouti, Adjunct Lecturer NTUA

Athens, 2026

Abstract

This diploma thesis addresses several core components of the design process, applied within the framework of the Fire Satellite (FS) case study, a widely used benchmark for Uncertainty Quantification (UQ) solvers in multidisciplinary systems. The domains covered are Multidisciplinary Analysis (MDA) and Optimization (MDO), Uncertainty Quantification, and Multidisciplinary Optimization under Uncertainty ($MDOuU$).

The FS is a conceptual Earth-observation system designed to detect and monitor fire events, from orbit. Its operation requires the coordinated interaction of subsystems governing orbital dynamics, power generation, and attitude control, making it an appropriate and representative test case for MDA. The FS case defines a set of key functions, termed Quantities of Interest (QoIs), which characterize system performance.

For the MDA, the Multidisciplinary Design Feasible (MDF) formulation is adopted, ensuring full iterative convergence of the entire MD system in each step.

Within the UQ framework, statistical moments are computed using the Method of Moments (MoM). This requires evaluation of the first- and second-order derivatives of the Quantities of Interest (QoI) with respect to the uncertain input variables. The derivatives are computed using Direct Differentiation and the Adjoint Method.

The subsequent $MDOuU$ formulates its objectives as weighted sums of the statistical

moments of the selected QoIs. Several optimization runs with varying weights generate a Pareto front for each QoI. The resulting MDO problem is solved using the gradient-based Steepest Descent method. The necessary sensitivity derivatives—both those associated with the functions of the underlying MD system and those arising from the UQ formulation—are computed using Finite Differences.

Εθνικό Μετσόβιο Πολυτεχνείο
Σχολή Μηχανολόγων Μηχανικών
Τομέας Ρευστών
Μονάδα Παράλληλης Υπολογιστικής

Ρευστοδυναμικής & Βελτιστοποίησης

Πολυπεδιακή Ανάλυση και Βελτιστοποίηση υπό Αβεβαιότητες. Εφαρμογή σε Δορυφόρο Παρακολούθησης Πυρκαγιών

Διπλωματική Εργασία

Βασιλειάδης Ορφέας Λάμπρος

Επιβλέποντες:

Κυριάκος Χ. Γιαννάκογλου, Καθηγητής ΕΜΠ

Δρ. Β. Ασούτη, Εντεταλμένη Διδάσκουσα ΕΜΠ

Αθήνα, 2026

Περίληψη

Η διπλωματική αυτή εργασία πραγματεύεται τρεις βασικούς τομείς σχεδιασμού, εφαρμοσμένους στο πλαίσιο του προβλήματος του Δορυφόρου Ανίχνευσης Πυρκαγιών (Fire Satellite - FS), ενός ευρέως χρησιμοποιούμενου προτύπου για τη δοκιμή επιλυτών Ποσοτικοποίησης Αβεβαιότητας σε ένα πολυπεδιακό σύστημα. Οι τομείς που καλύπτονται είναι η Πολυπεδιακή Ανάλυση (MDA) και Βελτιστοποίηση (MDO), η Ποσοτικοποίηση Αβεβαιότητας (UQ) και η Πολυπεδιακή Βελτιστοποίηση υπό Αβεβαιότητες ($MDOuU$).

Ο FS είναι ένα θεωρητικό σύστημα παρατήρησης της Γης, σχεδιασμένο για την ανίχνευση και παρακολούθηση περιστατικών πυρκαγιάς, από τροχιά. Η λειτουργία του απαιτεί τη συντονισμένη αλληλεπίδραση πολλαπλών πεδίων, συμπεριλαμβανομένων της τροχιακής δυναμικής, της παραγωγής ισχύος και του συστήματος ελέγχου προσανατολισμού, καθιστώντας το ένα κατάλληλο και αντιπροσωπευτικό δοκιμαστικό πρόβλημα για MDA. Το πρόβλημα FS ορίζει ένα σύνολο βασικών συναρτήσεων, γνωστών ως Μεγέθη Ενδιαφέροντος (QoIs), τα οποία χαρακτηρίζουν την απόδοση του συστήματος.

Για την MDA, υιοθετείται η διατύπωση Multidisciplinary Design Feasible (MDF), η

οποία εξασφαλίζει πλήρη σύγκλιση, μέσω επαναλήψεων, ολόκληρου του MD συστήματος σε κάθε βήμα.

Στο πλαίσιο της UQ, οι στατιστικές ροπές υπολογίζονται με χρήση της Μεθόδου Ροπών (MoM). Αυτό απαιτεί τον υπολογισμό των παραγώγων πρώτης και δεύτερης τάξης των Μεγεθών Ενδιαφέροντος (QoI) ως προς τις αβέβαιες μεταβλητές εισόδου. Οι παράγωγοι αυτές υπολογίζονται με χρήση Άμεσης Διαφόρισης (DD) και της Συζυγούς Μεθόδου (AM).

Η επακόλουθη $MDOuU$ διαμορφώνει τις αντικειμενικές συναρτήσεις ως σταθμισμένα αθροίσματα των στατιστικών ροπών των επιλεγμένων QoIs. Μερικά τρεξίματα της βελτιστοποίησης με μεταβαλλόμενα βάρη παράγουν ένα Μέτωπο Pareto για κάθε QoI. Το προκύπτον πρόβλημα MDO επιλύεται με χρήση της Αιτιοκρατικής Μεθόδου Απότομης Κλίσης (SD). Οι νέες απαιτούμενες παράγωγοι ευαισθησίας —τόσο των συναρτήσεων του βασικού MD συστήματος όσο και εκείνων που προκύπτουν από τη διατύπωση της UQ— υπολογίζονται με χρήση Πεπερασμένων Διαφορών (FD).

Abbreviations

ACS Attitude Control System

AM Adjoint Method

DD Direct Differentiation

FD Finite Difference

FS Fire Satellite

IDF Individual Discipline Feasible

LHS Latin Hypercube Sampling

MC Monte Carlo

MD Multidisciplinary

MDA Multidisciplinary Analysis

MDAuU Multidisciplinary Analysis under Uncertainty

MDF Multidisciplinary Design Feasible

MDO Multidisciplinary Optimization

MDOuU Multidisciplinary Optimization under Uncertainty

MoM Method of Moments

PDF Probability Density Function

QoI Quantity of Interest

SD Steepest Descent

UQ Uncertainty Quantification

XDSM Extended Design Structure Matrix

Contents

Chapter 1

Introduction

This diploma thesis addresses several domains of design process, applied within the framework of the Fire Satellite (FS) case study. These domains are:

- Multidisciplinary Analysis (MDA) & Optimization (MDO)
- Uncertainty Quantification (UQ) in an MD system
- Multidisciplinary Optimization under Uncertainty ($MDOuU$)

Multidisciplinary cases divide an analysis into separate sets of equations, called disciplines. Together, they capture the overall physics of a real-world system.

Realistically, the inputs that shape an analysis are rarely constant. Physical measures are characterized not by a single value, but by a range of values with certain probabilistic properties. UQ derives, given the probability density function of input parameters, the probabilistic qualities of a desired output function, or Quantity of Interest (QoI).

The following $MDOuU$ improves the robustness of the system, instead of targeting the minimization of a single function. The objectives become the first two statistical moments of the QoI, i.e its mean value μ and its standard deviation σ. The system must be designed so that the outcome is acceptable despite the variance of its inputs. A low mean value of a QoI may not be sufficient if accompanied by a large probabilistic variance.

The FS case, implemented to illustrate the analysis objectives described above, is a well-known framework for testing Uncertainty Quantification solvers in an MD system of equations. The case was taken from the *OpenTURNS* documentation [1] and is based on the combined works of Wertz [2], Sankaraman [3], and Zaman [4]. It provides a basic introduction to the initial analysis required for designing a satellite capable of detecting and tracking fires from orbit.

1.1 The Fire Satellite Case

The FS' primary objective is to autonomously navigate a fixed orbit while managing its power and orientation to ensure continuous operation and observation of target areas.

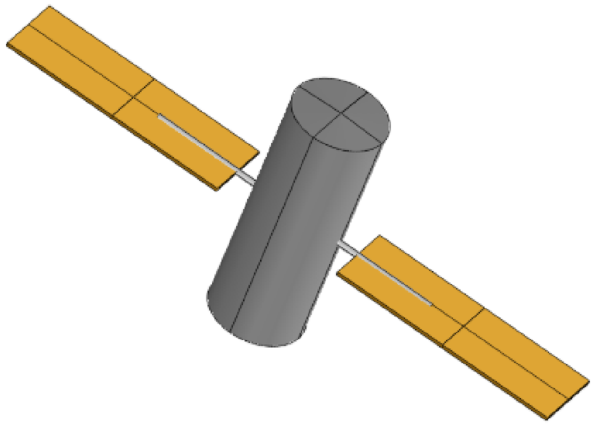

Figure 1.1: The FS model as presented in *OpenTURNS* [1].

The FS framework is presented qualitatively in Chapter 2, while the entire equation system is given extensively in Appendix A. The case consists of three separate sets of equations, referred to as disciplines:

- Orbit Mechanics
- Power Production
- Attitude Control System (ACS)

The satellite's orbit is shaped solely by the Earth's gravitational field. Its translational motion is assumed steady throughout the mission. The first discipline, *Orbit* Mechanics, calculates the parameters governing the satellite's motion.

Once the orbital parameters are determined, the next consideration is the satellite's power requirements. The second discipline, governing *Power* Production, evaluates the energy demands of the system and determines the appropriate sizing of the solar arrays to ensure that sufficient power is generated for continuous operation.

The satellite's angular orientation, or attitude, must then be controlled to fulfill operational objectives, such as orienting solar panels toward the Sun or pointing sensors at target areas. This task is handled by the *Attitude Control System* (ACS), the third discipline, which is coupled with the *Power* discipline due to its direct contribution to the satellite's energy consumption. The satellite uses a three-axis reaction wheel system to control its orientation. Reaction wheels operate on Newton's third law: applying a torque to spin a wheel in one direction induces an equal and opposite torque on the satellite's body, enabling precise maneuvering without propulsion. With a three-axis arrangement, all possible slewing motions are achievable.

The QoIs for the FS system are the solar array surface area A_{sa}, the total generated power P_{tot}—both evaluated within the second discipline—and the total disturbance torque τ_{tot}, evaluated within the third discipline. These metrics collectively characterize the system's performance in terms of energy generation, hardware sizing, and attitude stability.

In this framework there are inherently linked functions shared between disciplines, consequently named coupled. These are the moments of inertia I_{max} and I_{min}, and the attitude control power P_{ACS}. P_{ACS}, evaluated in the second discipline (*Power*), expresses the power required to maneuver the satellite and determines the sizing of the solar arrays. This sizing, in turn, affects the satellite's mass distribution and thus its moments of inertia I_{max} and I_{min}, which directly influence the torque requirements for attitude control, evaluated in the third discipline (*ACS*). These updated requirements feed back into the system, and the cycle repeats until convergence of the coupled functions' values is achieved.

1.2 Multi Disciplinary Analysis

The key word of MD cases is interdependency. Disciplines communicate with each other through common functions $Y_{i,j}$, in which i indicates the discipline of origin, and j indicates the receiving discipline. The $XDSM$ of Fig. 1.2 presents an example of a 3-discipline case.

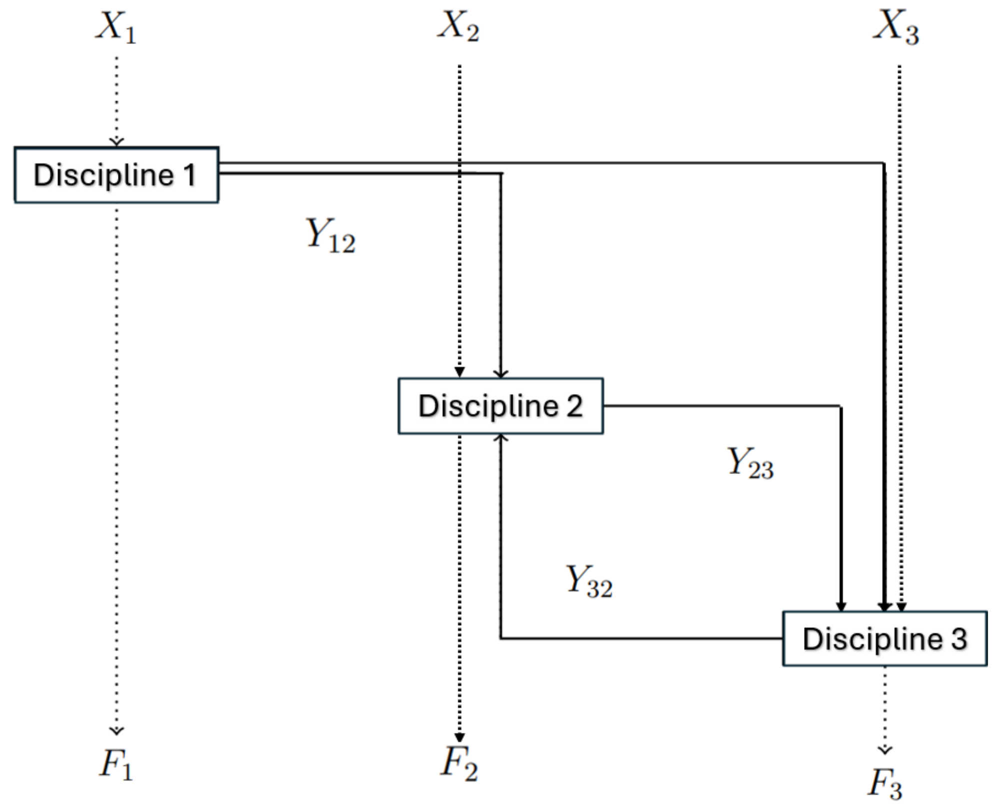

Figure 1.2: *MD* 3-Discipline Example Structure.

The system takes the variables X_i as input, where i denotes the discipline they govern. In some cases, there are global variables X, factoring in all disciplines. Using X_i and $Y_{j,i}$ as input, the outputs F_i of each discipline are evaluated. Different disciplines are solved co-dependently, as they exchange coupled functions $Y_{i,j}$. The system converges if the coupled functions are in equilibrium. In other words, multidisciplinary feasibility has been achieved. That is, the system has reached a meaningful state, that satisfies the disciplines, the physical constraints of the case. System feasibility, or convergence, is most commonly employed iteratively, using an informed initialization for the coupled functions.

1.3 Multi Disciplinary Optimization

MDO solvers are divided into two categories of architectures: Monolithic and Distributed. In this thesis, the case will be optimized using a Monolithic architecture, which means that a single, system-level optimization problem will be targeted.

There are two primary categories of optimization solvers: stochastic methods (often evolutionary algorithms, *EA*, [5]) and gradient-based methods. Evolutionary algorithms employ sophisticated search strategies to update the design variable vector at each iteration, typically following the evaluation of a computationally expensive population of samples. These methods rely solely on objective function evaluations, making them well suited for black-box systems where derivative information is unavailable.

Gradient-based methods are more direct as the computed gradient of the objective function leads the solver towards a descent direction of the objective function at every cycle. Thus convergence typically requires fewer cycles compared to the EA approaches. It also means that the result is reliant on the initialization, as an unfortunate initialization may drive the optimization to a local optimum, not the global. Fig. 1.3 shows the workflow of each optimization cycle.

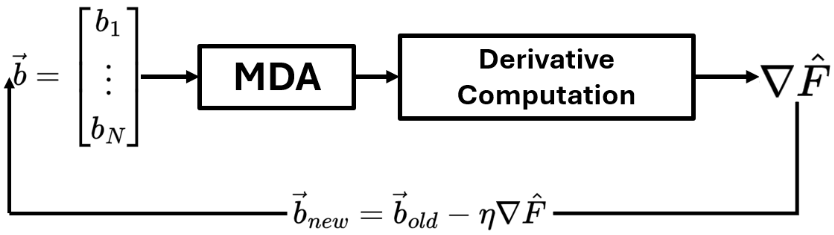

Figure 1.3: MDO Procedure.

Steepest descent (SD) will be implemented for the design variable update, which means that only the first-order derivatives with respect to the design variables will be needed. In the objective of minimization, SD updates the design variables in a step that is opposite to the derivative of the objective function:

$$\Delta \vec{b} = -\eta \nabla \hat{F}$$

$$\vec{b}_{new} = \vec{b}_{old} - \eta \nabla \hat{F}$$

The value of the scalar quantity η is experimented upon to ensure stable steps. Alternative methods ([6, 7]) would require higher-order derivatives of the objective function (like the Newton Method, which uses a quadratic Taylor approximation of the objective function and minimizes it), or their approximations using first derivatives (like the Quasi Newton Method, that can be implemented using a $BFGS$ approximation of the $Hessian$).

1.4 Uncertainty Quantification

UQ is implemented when the inputs of a system take on stochastic—or uncertain—values, rather than deterministic ones. In this thesis, the uncertain variables handled, denoted by $\vec{c} = \mathbf{c}$, follow normal distributions, with given mean values and standard deviations:

$$c_i = c_i(\mu_i, \sigma_i)\,, \quad \text{with} \quad i = 1, \cdots, M$$

The statistical moments of the QoI, i.e its mean value μ and its standard deviation σ, can be obtained either by sampling the uncertain space (whether the sampling is purely stochastic like the Monte Carlo method—MC, [8]—or set mathematically like the Gauss Quadrature method—GQ, [9]), or computationally, through the Method of Moments (MoM, [10]. The more stochastic the method, the higher its cost. Using the MoM, the statistical moments are obtained after a single feasible solution of the MDA.

$$\vec{c} = \begin{bmatrix} c_1(\mu,\sigma) \\ \vdots \\ c_M(\mu,\sigma) \end{bmatrix} \longrightarrow \boxed{\textbf{UQ}} \longrightarrow \vec{f} = \begin{bmatrix} f_1(\mu,\sigma) \\ f_2(\mu,\sigma) \\ f_3(\mu,\sigma) \end{bmatrix}$$

The first statistical moment is the expected value, the mean value of the QoI. That is obtained by averaging the function of interest F through the probability density function (PDF) $p(\mathbf{c})$, with $\mathbf{c}$ denoting the uncertain variable field:

$$\mu_F = \int_{-\infty}^{+\infty} F(\mathbf{c})p(\mathbf{c})d\mathbf{c}$$

The second statistical moment, the variance, is found by averaging the square of that same function around the mean value:

$$\sigma^2 = \int_{-\infty}^{+\infty} (F(\mathbf{c}) - \mu_F)^2 p(\mathbf{c})d\mathbf{c}$$

For the integrals to be computed using the MoM, the Taylor expansion of the function is used, expressed around the state vector $\bar{\mathbf{c}}$, i.e the vector of the mean values of all the uncertainties. Finally, the statistical moments are derived. Appendix B shows the proof of the formulas presented below:

$$\begin{aligned} \mu_F &= F\big|_{\bar{\mathbf{c}}} + \frac{1}{2}\sum_{i=1}^{M} \frac{d^2F}{dc_i^2}\bigg|_{\bar{\mathbf{c}}} \sigma_i^2, \\ \sigma_F^2 &= \sum_{i=1}^{M} \left(\frac{dF}{dc_i}\right)^2\bigg|_{\bar{\mathbf{c}}} \sigma_i^2 + \frac{1}{2}\sum_{i=1}^{M}\sum_{j=1}^{M} \left(\frac{d^2F}{dc_i dc_j}\right)^2\bigg|_{\bar{\mathbf{c}}} \sigma_i^2\sigma_j^2. \end{aligned} \tag{1.1}$$

It is clear that the first- and second-order derivatives of the QoI with respect to the uncertain variables must be evaluated. The expressions presented above are based on a second-order Taylor expansion; however, the same procedure extends directly to higher-order expansions, although the results are typically sufficiently accurate at second order. Let it be noted that probability distributions other than the normal distribution can be treated within the same framework without modification of the overall approach.

1.5 MDO under Uncertainties

The objective of the analysis is the simultaneous minimization of both the mean value and the standard deviation of each QoI. This reflects the requirement not only for optimal performance on average, but also for robustness against uncertainty. A design with a low mean value but high variability may lead to unreliable operation, while a design with slightly higher mean performance but low variability may be preferable in practice. The objective function $\hat{F}$ will be a weighted sum of the statistical moments of the QoI in question:

$$\hat{F} = k\ \mu_F + (1-k)\sqrt{\sigma_F^2} \quad , \quad \text{where} \quad k \in [0,1].$$

This way, multiple runs of the optimization using different weights k can provide a set of optimal solutions. Experimenting with a whole range of values for k, a Pareto Front can be computed, providing the engineer with a set of probabilistic qualities for the QoI. Employing gradient-based methods, the derivatives of the objective function are essential:

$$\frac{d\hat{F}}{db_l} = k\frac{d\mu_F}{db_l} + (1-k)\frac{d\sqrt{\sigma_F^2}}{db_l}$$

Substituting Eqs. 1.1 stated in the UQ introduction, the objective function's derivatives with respect to the design variables $\vec{b}$ would be:

$$\frac{d\hat{F}}{db_l} = k\left(\frac{dF}{db_l} + \frac{1}{2}\frac{d^3F}{dc_i^2 db_l}\sigma_i^2\right) + (1-k)\frac{2\frac{dF}{dc_i}\frac{d^2F}{dc_i db_l}\sigma_i^2 + \frac{d^2F}{dc_i dc_j}\frac{d^3F}{dc_i dc_j db_l}\sigma_i^2\sigma_j^2}{2\sqrt{\left[\frac{dF}{dc_i}\right]^2\sigma_i^2 + \frac{1}{2}\left[\frac{d^2F}{dc_i dc_j}\right]^2\sigma_i^2\sigma_j^2}}$$

The UQ subproblem is solved for every optimization cycle to obtain the values of the statistical moments of the QoI.

1.6 Thesis Outline

Having introduced all components of this thesis' design analysis, the FS case study can be addressed. The system is examined to characterize the behavior of the QoIs both in terms of their baseline response to uncertain inputs and under the robust design formulation.

The benchmark FS equation system is detailed in Chapter 2, where the QoIs are defined and the physical interpretation of the coupling between disciplines is discussed.

Chapter 3 presents the MDA framework built to solve the FS case to obtain the values of the QoIs, along with the methods subsequently employed to optimize them.

Building upon the foundation of the MDA, the probabilistic characteristics of the QoIs are subsequently quantified through the UQ analysis of Chapter 4, allowing the impact of uncertainties in model inputs to be assessed. The MoM provides the statistical moments of the QoIs which are essential for evaluating system reliability.

Finally, the QoIs are incorporated into the gradient-based MDO framework of Chapter 5, where they are optimized according to the selected robustness criteria. The optimization objective is to achieve a balance between performance and reliability, typically formulated as a trade-off between the mean values of the QoIs and their associated variability, ensuring solutions that are not only optimal under nominal conditions but also resilient to uncertainty.

Chapter 2

The Fire Satellite Case

This chapter provides a description of the disciplines involved in the MD case, with emphasis on their formulation and interactions within the overall framework. The formulation of the equations assumes deterministic values for all inputs. In later chapters, certain inputs are treated as uncertain; however, the MD system itself is always solved for a single realization of the inputs. The formulas are presented extensively in Appendix A, along with Table A.1 providing all used deterministic measures.

2.1 Primal Equations' System

Discipline 1 - Orbit Mechanics

The first discipline governs the physics of the satellite's translational motion. The satellite is designed to operate in a *Medium Earth Orbit* at an altitude of $H = 18 \times 10^3$ km. According to Newton's law of universal gravitation [11], maintaining this orbital altitude requires the FS to travel at a velocity given by:

$$V = \sqrt{\frac{GM_{earth}}{R_{earth} + H}} \tag{2.1}$$

where the product GM_{earth} is Earth's gravity constant. This gives a velocity of about $V \simeq 4000\ ms^{-1}$. Under this steady velocity, the satellite's circular orbit is characterized by a period of:

$$\Delta T_{orbit} = 2\pi \sqrt{\frac{(R_{earth} + H)^3}{GM_{earth}}} \tag{2.2}$$

which is about $10\frac{1}{2}$ hrs. Approximating the Earth's shadow as a cylindrical space, the eclipse part duration of the satellite's orbit is calculated as:

$$\Delta T_{eclipse} = \frac{\Delta T_{orbit}}{\pi} \arcsin\left(\frac{R_{earth}}{R_{earth} + H}\right) \tag{2.3}$$

that is about 50 $mins$. The information of the two durations—the total orbit period ΔT_{orbit} and the time not illuminated by the Sun, $\Delta T_{eclipse}$—is crucial to shape the power production requirements, addressed in discipline 2 (*Power*).

Before moving on, there is another important function that shapes the analysis: knowing the orbit altitude H and the targeted Earth surface area covered by the satellite's scope $\varnothing_{target}$, the reference slewing angle (Appendix A) is:

$$\theta_{slew} = \arctan\left(\frac{\sin\phi}{1 - \cos\phi + \frac{H}{R_{earth}}}\right) \tag{2.4}$$

where ϕ is the central angle subtended at the center of the Earth:

$$\phi = \frac{Arc}{Radius} = \frac{\varnothing_{target}}{2R_{Earth}} \tag{2.5}$$

The target diameter $\varnothing_{target}$ is set, by the case, to 235 km, which corresponds to approximately 0.59% of the Earth's circumference.

The values of V and θ_{slew} act then as inputs to discipline 3, of the *Attitude Control System* (ACS). These measures are crucial to realize the disturbances acted on the satellite, and the required swerving it will perform.

Discipline 2 - Power Production

The second discipline calculates the required power needed for the satellite swerving motions, as well as the means to produce it using its solar arrays. The equations governing this discipline are less physically explicit than those of the preceding one; therefore, only the key computations are presented. Firstly, the total power, which determines the requirements of the ACS as well as additional operational needs, is calculated as:

$$P_{tot} = P_{ACS} + P_{other} \tag{2.6}$$

Knowing the total power demands P_{tot} and accounting for the eclipse portion of the orbit, during which no power is generated, the required power produced by the solar panels is:

$$P_{sa} = P_{tot} \frac{\frac{\Delta T_{eclipse}}{0.6} + \frac{T_{sunlight}}{0.8}}{T_{sunlight}} \tag{2.7}$$

The required solar array area is then computed based on its power generation capability (expressed in $W\,m^{-2}$):

$$A_{sa} = \frac{P_{sa}}{P_{cap}} \tag{2.8}$$

The second discipline therefore concludes by computing the satellite's moments of inertia. Knowing the arrangement of the solar panels, they are found by using their total size:

$$I_x = I_x(A_{sa}), \quad I_y = I_y(A_{sa}), \quad I_z = I_z(A_{sa})$$

Discipline 3 - Attitude Control System (ACS)

The third discipline handles input functions from the other disciplines, and uses them to compute measures of attitude disturbances and the respective torque requirements. The satellite velocity (from discipline 1) and its moments of inertia (from discipline 2), along with other local input parameters, formulate disturbing torque equations that need to be overcome. These torques are truly infinitesimal in value, with magnitudes on the order of $\mathcal{O}(10^{-6})$–$\mathcal{O}(10^{-5})$ Nm, but in orbit, they amount to concerning results.

Aerodynamic Torque

The infinitesimal value of the air density ρ is countered with the square of V, so the drag force is something to account for. Multiplying with the moment arm L_a, the torque is obtained:

$$\tau_{drag} = \frac{1}{2} L_a C_d \rho A V^2 \tag{2.9}$$

Gravity Gradient Torque

This torque is a key component of the analysis, as it captures the combined effect of a stabilizing gravitational interaction and the influence of the satellite's moments of inertia, I_{max} and I_{min}, computed in the previous discipline. It arises from the action of the gravitational field on a non-spherical body, leading to a tendency to align its principal axis toward the Earth. It is worth noting that this gravity-gradient torque also exists at a larger scale at the Earth's surface; however, its effect there is negligible compared to other dominant forces.

$$\tau_{g,max} = \frac{3GM_{earth}}{2\left(R_{earth} + H\right)^3}\left(I_{max} - I_{min}\right)\sin 2\theta \tag{2.10}$$

The angle θ is defined between the satellite's principal axis and the zenith direction, i.e., the radial line from the Earth. Depending on the design state, the term $(I_{max} - I_{min})$ may be expressed in terms of different inertia components. This leads to six possible combinations, reliant on the relative magnitudes of I_x, I_y, and I_z within the local coordinate system.

Solar Radiation Torque

This torque is generated by the satellite's interaction with the electromagnetic field of the sun. The exposure of the satellite to the Sun's radiation amounts to a physical, mechanical force acted on its surface by the bombardment of the Sun's photons. Similarly to the aerodynamic drag, a torque is produced—although the surface areas considered are not the same. The torque is then:

$$\tau_{sp} = L_{sp}\frac{F_s}{c}A_s\left(1 - q\right)\cos^2 i \tag{2.11}$$

where F_s is the average solar flux measured in Wm^{-2}, q is the reflectance factor of the panels, c is the speed of light, A_s is the area reflecting radiation and finally i is the angle between the panels' normal vector and the solar rays.

Magnetic Field Interaction Torque

The satellite is composed of metal parts, that over long exposure in the Earth's magnetic field can get magnetized to an alarming point. If left unchecked, the satellite will align with the magnetic lines of the Earth and will be rendered unable to escape their direction. The torque is equal to:

$$\tau_m = \frac{\mu_0}{4\pi}\frac{2MR_D}{\left(R_{earth} + H\right)^3} \tag{2.12}$$

where M is the Earth's magnetic moment measured in Am^2, a measure that represents the strength and orientation of the Earth's global magnetic field, and R_D, also measured in Am^2, is the unintended magnetic moment of the satellite, its residual dipole. The constant μ_0 denotes the permeability of free space, measured in $\mathrm{N\,A^{-2}}$.

Total Disturbing Torque

The disturbing torques are collected into one measure quantifying their influence:

$$\tau_{dist} = \sqrt{\tau_{drag}^2 + \tau_g^2 + \tau_{sp}^2 + \tau_m^2} \tag{2.13}$$

Slewing Torque

In addition to the disturbing torques that the satellite must counteract, the FS framework defines a target torque that further tightens the ACS requirements. The slewing torque represents the maximum torque that the ACS must generate to reorient the satellite, either to direct its sensor toward a new target or to align its solar panels with the Sun. The maneuver is defined over a reference angle, denoted θ_{slew}, which characterizes the required reorientation.

$$\tau_{slew} = I_{max} \frac{4\theta_{slew}}{\Delta t_{slew}^2} \tag{2.14}$$

Again, a moment of inertia surfaces in the calculations. To ensure a conservative estimate, the largest moment of inertia is used, no matter the local x, y, z coefficient it belongs to.

Total Torque

Having discussed each torque accounted for, the final step before this discipline concludes, is the evaluation of these measures. The final, total torque required by the ACS, is then:

$$\tau_{tot} = \max(\tau_{slew}, \tau_{dist}) \tag{2.15}$$

This formulation dictates that there are multiple routes to the system, depending on the inputs. There are actually nine possible scenarios that can arise in the design analysis, all covered in Appendix A. Once the total torque has been determined from the ACS discipline, the corresponding attitude control power can be calculated:

$$P_{ACS} = \tau_{tot}\omega_{max} + 3P_{hold} \tag{2.16}$$

Simply put, based on the demands the moments of inertia have on the ACS, the power needed is computed. The key point is that the satellite's moments of inertia strongly influence the total torque required from the ACS, which in turn determines the power production requirements. As a result, Disciplines 2 and 3 are coupled in their evaluations.

2.2 Model Interpretation

Having established the FS framework, it becomes clear why it provides a suitable foundation for an MDA. The key aspects of translational motion, rotational dynamics, and power generation are decomposed into distinct disciplines, allowing different physical domains to interact and collectively define the overall system behavior and outputs.

The QoIs for the FS system are the solar array surface area A_{sa}, the total generated power P_{tot}—both evaluated within the second discipline—and the total required torque τ_{tot}, evaluated within the third discipline. These metrics collectively characterize the system's performance in terms of energy generation, hardware sizing, and attitude stability.

The baseline FS configuration yields a solar array sizing of approximately $A_{sa} = 10\,\mathrm{m}^2$, a measure representative of a configuration designed to sustain moderate onboard power requirements while accounting for eclipse phases. This corresponds to a total power demand of about $P_{tot} = 1100$ W, typical for these kinds of operations. The torque requirement is also relatively low, demanding about $\tau_{tot} = 0.01$ Nm for the satellite attitude control. It is clear that the ACS is primarily compensating for small disturbance torques and performing modest reorientation maneuvers rather than aggressive slewing.

Each QoI plays a distinct and competing role in the system design. The solar array area A_{sa} directly impacts the satellite's mass and structural requirements, making its minimization desirable from a design perspective. The total power P_{tot} determines the system's operational capability and must remain sufficiently high to satisfy all subsystem demands. The disturbance torque τ_{tot} influences the performance of the attitude control system, as higher torques require greater control effort and increased energy consumption. These objectives are inherently coupled. For instance, increasing the solar array area may improve power generation but also amplifies disturbance torques due to larger exposed surfaces. As a result, the design problem is not one of independent optimization, but of balancing competing effects. The role of the QoIs is therefore central, as they define both the performance metrics and the trade-offs that govern the overall system behavior.

The coupled functions of the system are the attitude control power P_{ACS} and the moments of inertia I_{max} and I_{min}. These quantities are inherently interdependent: their values are obtained simultaneously as the system converges. P_{ACS}, evaluated in the Power discipline, expresses the required power to maneuver the satellite, and thus determines the sizing of the solar arrays. This sizing, in turn, affects the satellite's mass distribution and consequently its moments of inertia I_{max} and I_{min}, which directly influence the torque requirements for attitude control, evaluated in the ACS discipline. These updated requirements feed back into the system, and the cycle between disciplines 2 and 3 repeats until convergence of the coupled functions' values is achieved.

2.2.1 Uncertain Inputs and Uncertainty Propagation

While the equation system is presented in a deterministic manner, with fixed values assigned to all inputs, such an assumption does not fully reflect the nature of the case. In practice, many of these parameters are subject to uncertainty and variability, arising from modeling assumptions, environmental conditions, and physical limitations. For instance, although a target orbital altitude H may be prescribed, it cannot be considered strictly constant, as the motion does not occur between idealized bodies; deviations from perfect spherical symmetry and external perturbations introduce variations in the actual trajectory. Similarly, the variability in satellite orientation induced by constant or oscillatory disturbances cannot be adequately evaluated without accounting for uncertainty. Quantities such as the moment arms L and the effective surface areas A, which contribute to several torque components, depend on the satellite's orientation, and must therefore be treated as varying parameters within the analysis.

Consequently, a realistic treatment of the system requires acknowledging and incorporating these and many other uncertainties. The uncertain input variables are introduced in detail in the UQ Chapter 4, along with the handling of the uncertainty propagation through the system, that ultimately shapes the QoIs' nature of variability.

Chapter 3

MDA-MDO

The FS equation system has been established. This chapter presents the solution of the MDA and the subsequent MDO. In the MDA, all inputs are treated as deterministic, as within a single execution of the MDA, even uncertain parameters are represented by fixed values until convergence of the system is achieved. The objective is to highlight the interdependencies within the MD system.

3.1 MDA

Each discipline receives input variables denoted by X, whether local or global, deterministic or uncertain. The QoIs are represented through the output functions F—for the disciplines that do compute them. The inter-discipline functions, which act both as inputs and outputs, are denoted by $Y_{i,j}$ or $Y_{k,i}$ depending on their direction, i.e., whether they are provided to or received from another discipline.

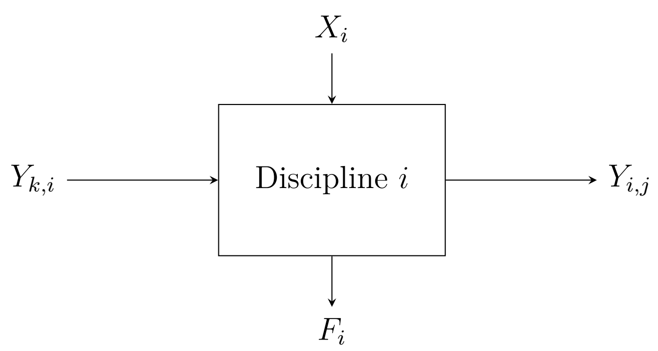

Figure 3.1: Individual Discipline Inputs and Outputs

Every discipline receives inputs gathered from the orbit conditions. The *Orbit* discipline feeds functions to the other disciplines, and receives none in return. It also does not offer a *QoI* as output.

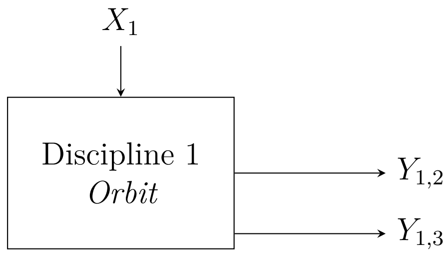

Figure 3.2: Discipline 1 Inputs and Outputs

The *Power* discipline receives functions from both other disciplines, and feeds the moments of inertia to the third discipline. It also computes the *QoI*s A_{sa} and P_{tot}.

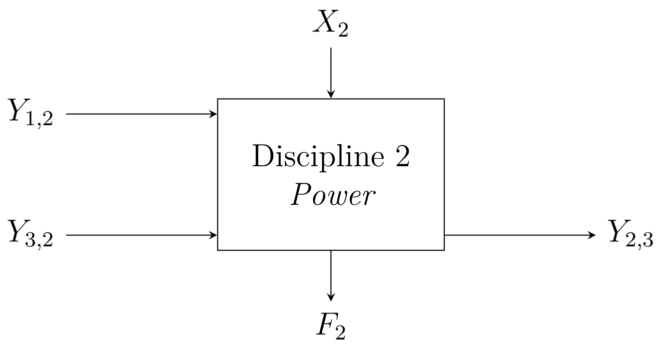

Figure 3.3: Discipline 2 Inputs and Outputs

The *ACS* discipline works similarly to the *Power* discipline: it receives input functions from both other disciplines, and sends the power needed for the *ACS* back to the second discipline. It offers the *QoI* τ_{tot}.

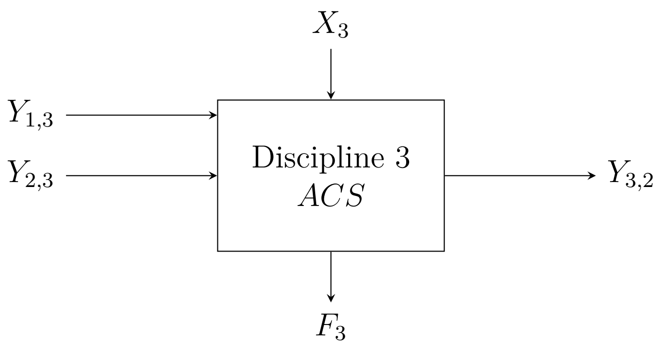

Figure 3.4: Discipline 3 Inputs and Outputs

The *MDA* framework has been established. Next step is to formulate the *UQ* and *MDO* processes that build upon it. There are methods that directly solve the *MD* system until convergence before proceeding to the next step, and others that perform only partial convergence around the solution, as discussed later.

For the UQ, the MDF formulation is a given, since there are no cycles of variable updates. Convergence measures must be used for the UQ to be reliable. Following an informed initialization of the coupled functions exchanged between disciplines 2 and 3, the system is iterated between the two disciplines to the point of convergence. The solution procedure of the MDA is shown in Algorithm 1.

Algorithm 1 Iterative Multidisciplinary Analysis Procedure

Solve **Orbit Discipline (1)** to obtain

$$\vec{Y}_{1,2} \equiv \{\Delta T_{orbit}, \Delta T_{eclipse}\}$$
$$\vec{Y}_{1,3} \equiv \{\theta_{slew}, V\},$$

Initialize $Y_{3,2} \equiv P_{ACS}$, $\vec{Y}_{2,3} \equiv \{I_{max}, I_{min}\}$
Set convergence tolerance ε «
repeat
    Store previous values $\vec{Y}^{old}_{2,3}$, $Y^{old}_{3,2}$
    Solve **Power Discipline (2)** for current P_{ACS}
    Update I_{max}, I_{min}
    Solve **ACS Discipline (3)** for updated I_{max}, I_{min}
    Update P_{ACS}
    Store new values $\vec{Y}^{new}_{2,3}$, $Y^{new}_{3,2}$
until $|Y^{old}_{3,2} - Y^{new}_{3,2}| < \varepsilon \ \wedge \ |\vec{Y}^{old}_{2,3} - \vec{Y}^{new}_{2,3}| < \varepsilon$

The convergence of the primal set of equations generally requires up to four iterations to achieve a tight tolerance.

3.1.1 Derivative Computation

The objective is the computation of the QoIs' total derivatives. Since the QoIs to be differentiated, as was presented in the previous chapters, are functions of the input variables $\vec{x}$ and of the coupled functions I_{max}, I_{min} and P_{ACS}, which will now be denoted as $Y_i, i = 1, \ldots, N_Y$:

$$\vec{f} = \vec{f}(\vec{x}, \vec{Y}(\vec{x}))$$

That means the derivatives with respect to $\vec{c}$ will be:

$$\frac{d\vec{f}}{d\vec{x}} = \frac{\partial \vec{f}}{\partial \vec{x}} + \frac{\partial \vec{f}}{\partial \vec{Y}} \frac{d\vec{Y}}{d\vec{x}} \tag{3.1}$$

To calculate the derivatives of the QoIs, a residual function (R_i) is then extracted for each of the coupled functions, forming a system the exact same way it would be formed for a single-discipline case, with the coupled functions being treated as state variables. Feasibility requires that the residuals be zero, together with all their higher-order derivatives:

$$\vec{R}(\vec{x}, \vec{Y}(\vec{x})) = 0, \qquad \frac{d\vec{R}}{d\vec{x}} = \frac{\partial \vec{R}}{\partial \vec{x}} + \frac{\partial \vec{R}}{\partial \vec{Y}} \frac{d\vec{Y}}{d\vec{x}} = 0 \tag{3.2}$$

The residuals of the FS case are defined by the MD equation system: Eqs. A.30 provide the residuals of all three moments of inertia, factoring in the Power discipline, and Eq. A.20 provides the residual of the ACS power demand P_{ACS}. The residuals factoring in the derivative analysis may vary depending on the case state, based on the torque criterion 2.15. Using, for instance, the scenario of $\tau_{tot} = \tau_{dist}$, with $I_{max} = I_x$ and $I_{min} = I_z$, the extracted residuals are:

$$\begin{aligned} R_1 &= I_{sa,X} - m_{sa}\left(\frac{1}{12}\left(L^2 + t^2\right) + \left(D + \frac{L}{2}\right)^2\right) = 0 \\ R_2 &= I_{sa,Z} - m_{sa}\left(\frac{1}{12}\left(L^2 + W^2\right) + \left(D + \frac{L}{2}\right)^2\right) = 0 \\ R_3 &= P_{ACS} - \tau_{tot}\omega_{max} - 3P_{hold} = 0 \end{aligned} \tag{3.3}$$

In this case, the size of the residual vector is $N_Y = 3$. Solving Eq. 3.2 for the coupled functions' derivatives, there arises a system of $N_Y \times N_Y = 3 \times 3$:

$$\frac{d\vec{Y}}{d\vec{x}} = -\left(\frac{\partial \vec{R}}{\partial \vec{Y}}\right)^{-1} \frac{\partial \vec{R}}{\partial \vec{x}} \tag{3.4}$$

Substituting to Eq. 3.1, the entire system of operations is acquired:

$$\frac{d\vec{f}}{d\vec{x}} = \frac{\partial \vec{f}}{\partial \vec{x}} - \frac{\partial \vec{f}}{\partial \vec{Y}} \left(\frac{\partial \vec{R}}{\partial \vec{Y}}\right)^{-1} \frac{\partial \vec{R}}{\partial \vec{x}} \tag{3.5}$$

Every partial derivative term presented above is easily extracted by the baseline equation system, while the total derivatives must be computed as presented. It should be noted that the system defined in Eq. 3.4 is sufficiently small (≤ 3) to be solved analytically. The MDF procedure is presented using the $XDSM$ of Fig. 3.5. In this formulation, system feasibility is ensured by driving the residuals to zero and, subsequently, the coupled derivative system arising from Disciplines 2 and 3 is solved.

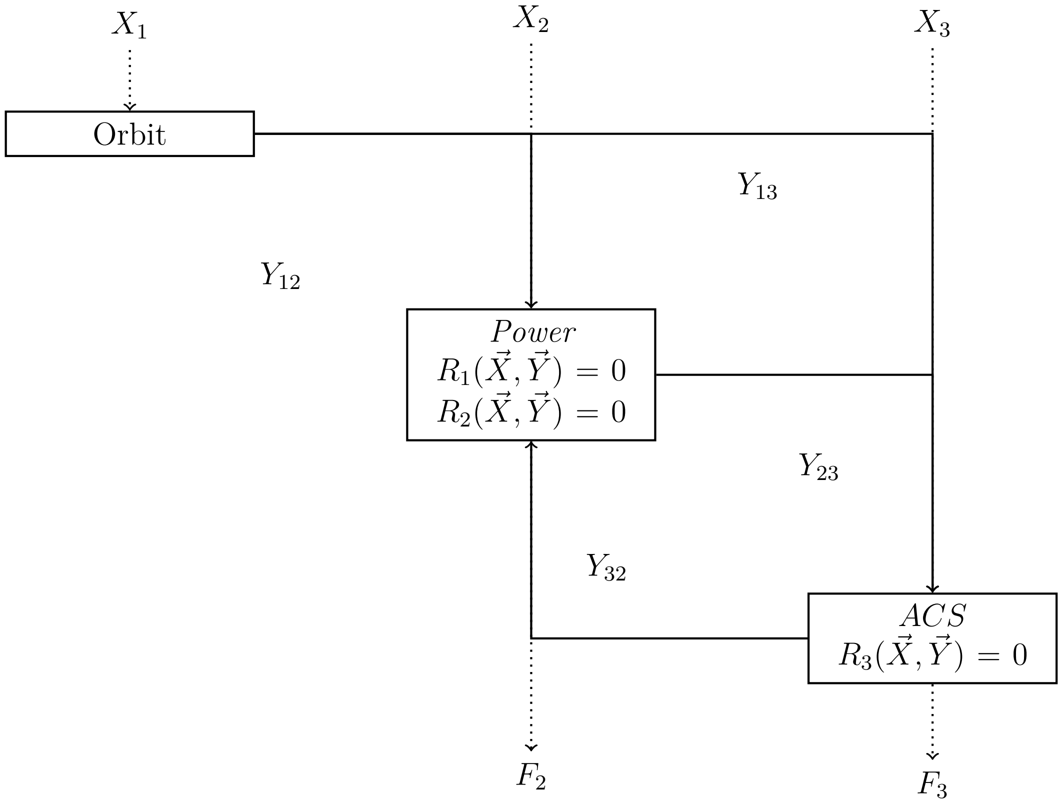

Figure 3.5: MDF for the FS.

Appendix C presents the decomposition of the MD system to extract the residuals and the computation of the total derivatives of the QoIs. These derivatives can be obtained either by explicitly differentiating the coupled functions, following the Direct Differentiation (DD) approach, or by bypassing them through the Adjoint Method (AM). The derivations are illustrated through the specific example of up-to-second-order derivatives of the QoIs with respect to the system uncertain inputs **c**. Although the appendix is framed within the context of UQ, where these derivatives are used to construct the MoM formulations in Chapter 4, the underlying procedure is general and directly applicable to the present MD analysis. At this stage, the uncertain variables are not treated probabilistically but rather as generic sensitivity variables, allowing the focus to remain on the computation of system-level derivatives. The results of the UQ, built upon these derivatives, are presented separately in Chapter 4.

When the straightforward MDF approach is not employed, an optimizer is introduced, tasked with working around the system convergence by approximating the same results. Different optimizers are discussed in the following section.

3.2 MDO

In the MDO, selected deterministic parameters from the baseline formulation are redefined as design variables and assigned admissible ranges consistent with the physical constraints of the problem. It is important to note that the baseline FS case is formulated as an $MDAuU$ framework rather than an optimization problem.

3.2.1 MDO Methods

The optimization is built using a Monolithic Architecture: the optimization of the MD system is approached system-wide, solving for a single objective, the same way as implemented for a single-discipline case. Distributed Architectures ([12, 13]) decompose the objective into discipline-specific optimization subproblems, with system-level variables or consistency targets employed to coordinate the disciplines. An admissable MDO architecture must remain mathematically equivalent to the original problem and thus converge to the same optima. The field of MDO approaches is vast and the literature provided in biblbiography ([14, 12, 13]) provides valuable insights and efficiency conclusions for a plethora of methods.

Monolithic Architecture Examples

The Multidisciplinary Design Feasible (MDF) enforces overall system feasibility: the system is converged for every step of the analysis, which may be a costly procedure for large systems. This ensures the system-level states to be physically compatible if the optimization stops prematurely.

The Individual Design Feasible (IDF) evaluates the disciplines separately, using target values for the coupled functions that control the stability of the system. The optimizer performs an iterative search for acceptable target values, a process which can make this method highly costly; however, this way the various disciplines can be solved in parallel, a crucial advantage for larger systems. If the iterative process is terminated prematurely, the resulting solution may remain infeasible, as consistency between the coupled variables has not yet been fully enforced.

The Simultaneous Analysis and Design ($SAND$) works similarly to an IDF solver, by-passing the evaluation of the MDA, by using the partial derivatives of the residuals, rather than being reliant on the total case derivatives. The $SAND$ architecture has the potential for being the most efficient way to get to the optimal solution, because it basically solves for all variables simultaneously. In practice, however, it is unlikely that this is advantageous when efficient component solvers are available.

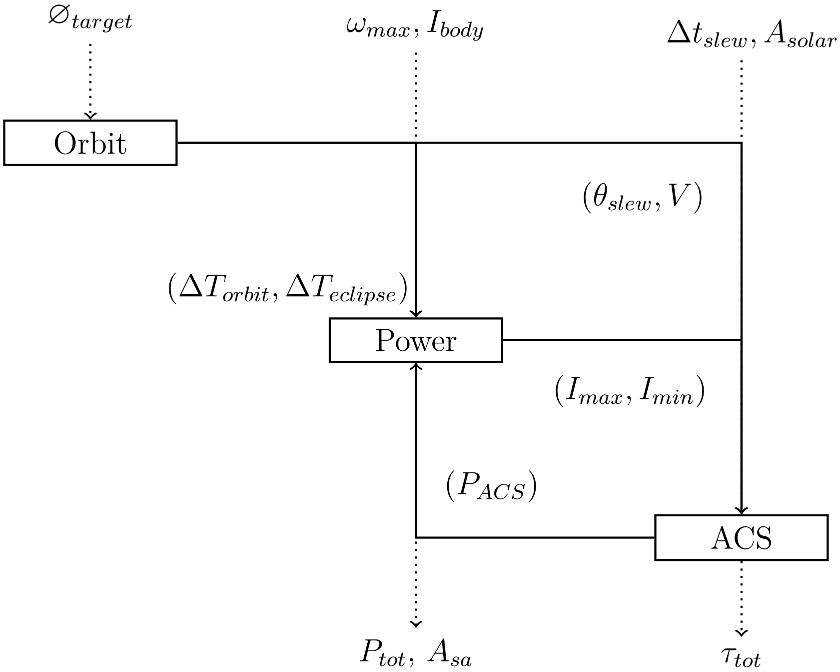

Figure 3.6: $XDSM$ of the FS case.

Distributed Architecture Examples

Collaborative Optimization (CO) solves the optimization subproblems independently, while satisfying local constraints for the individual discipline feasibilities. This method suffers from numerical ill-conditioning. Analytical Target Cascading (ATC) differs from CO in that it enforces penalties instead of constraints. Bilevel integrated system synthesis ($BLISS$) uses a series of linear approximations to the original design problem. These approximations are constructed at each iteration using coupled derivatives, which require an MDA evaluation. This makes $BLISS$ a distributed MDF architecture. Martins ([14]) concludes that unless a problem has a special structure, there is no distributed architecture that converges as rapidly as a monolithic one. In practice, distributed architectures have not been used much.

3.2.2 The MDO for the FS case

In this thesis, a Monolithic MDF Architecture is employed: at each optimization cycle, the entire MD system converges according to a tight tolerance, and then the solver proceeds, using the converged, feasible function values. The $XDSM$ of Fig. 3.6 presents the dependencies of the case, showing as inputs several key characteristic variables related to orbit mechanics, power consumption, and power production. All measures that can be introduced in the design space are given in Table A.1 of Appendix A.

Following the brief reference to the derivative computation outlined in Appendix C, attention is returned to the design space of the MDO problem. The chapter concludes with an overview of the practical aspects of the optimization process. Detailed runs and the corresponding result analysis are handled in the following chapters.

3.2.3 Identification of the Design Variables

Variables associated with all three disciplines are incorporated into the design space, resulting in a design variable vector that is not naturally well-conditioned, as it combines quantities of fundamentally different physical nature and scale:

$$\vec{b}_{\text{Orbit}}^T = \left[\varnothing_{target}\right]$$

$$\vec{b} = \begin{bmatrix} \vec{b}_{\text{Orbit}} \\ \vec{b}_{\text{Power}} \\ \vec{b}_{\text{ACS}} \end{bmatrix} \quad \text{, where} \quad \vec{b}_{\text{Power}}^T = \begin{bmatrix} \omega_{max} & P_{hold} & \epsilon_{deg} & LT & \eta_{bol} \\ Id & i & r_{lw} & \rho_{sa} & D \\ t & I_{body,X} & I_{body,Y} & I_{body,Z} & \end{bmatrix} \tag{3.6}$$

$$\vec{b}_{\text{ACS}}^T = \left[\Delta t_{slew} \quad A_{solar} \quad A_{air}\right]$$

Within this framework, the optimization is performed by selecting one QoI at a time.

An Insight Into A_{sa}

For this example, the convergence of the QoI A_{sa} is evaluated when each of the other two $QoIs$ is used as the objective function. That is to highlight the importance of prioritizing in each QoI, as even though they are coupled, they must be examined independently.

When the objective function of P_{tot} or τ_{tot} is minimized, A_{sa} does not tend to reduce along with the other objective functions. That is because of the crucial role A_{sa} plays in the formation of the values of the moments of inertia, which in turn define the magnitude of the gravity gradient torque as expressed in Eq. A.13. The optimization leads the A_{sa} to take on a value that minimizes P_{tot} or τ_{tot}.

Eqs. A.30 shows that the moments of inertia are expressions of various powers of A_{sa}. That leads to interesting relations between these functions. The values of the moments of inertia themselves do scale with A_{sa}, but the deviations between the maximum and the minimum, given by the term $(I_{max} - I_{min})$ do not necessarily. Figs. 3.7 are plots of the moments of inertia varying with respect only to A_{sa}, considering every design variable fixed, to highlight this relation.

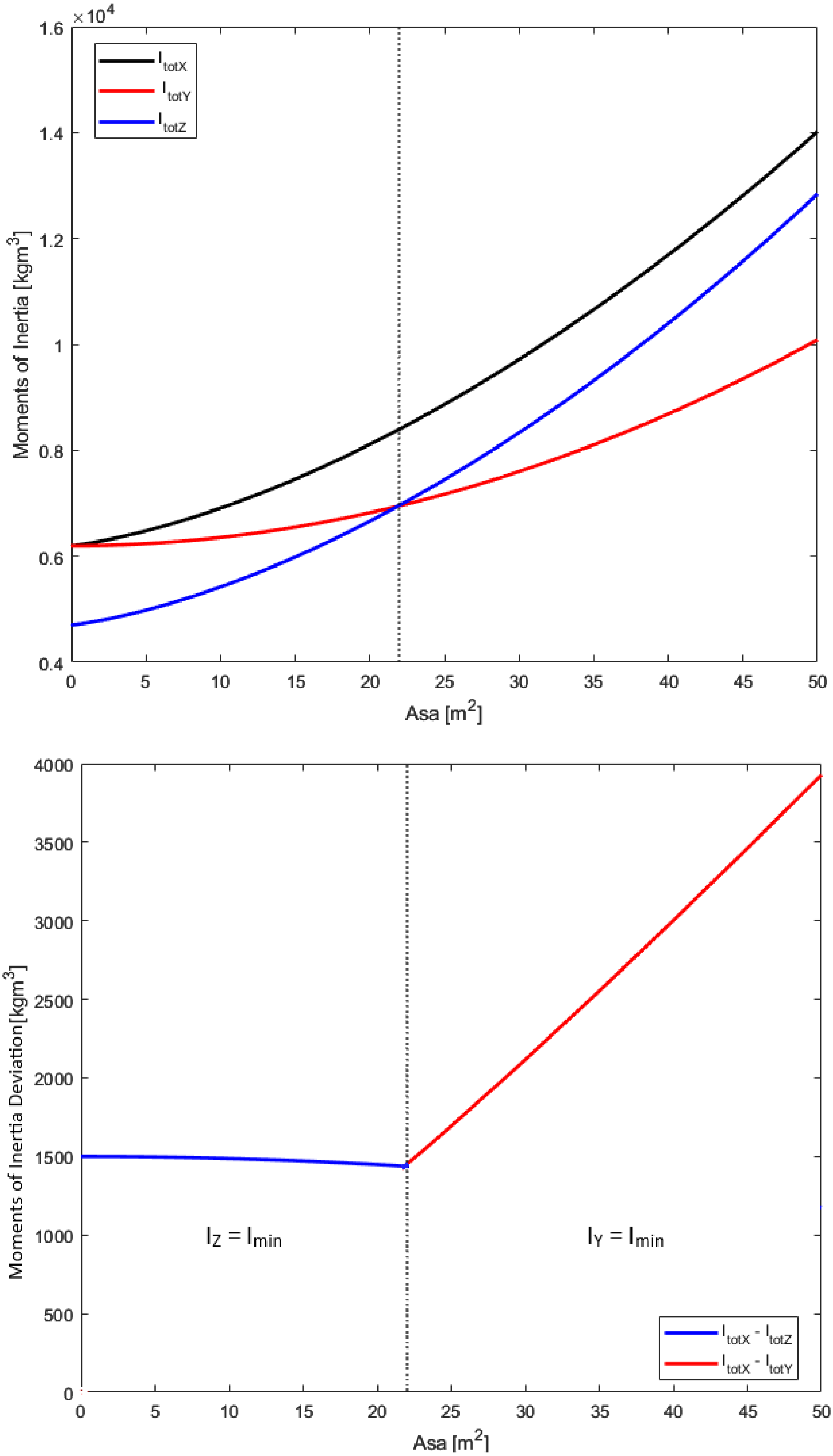

Figure 3.7: Moments of Inertia (only) with respect to A_{sa}.

In the first half of the plot, $I_z = I_{min}$. The term $(I_{max} - I_{min}) = I_x - I_z$ is inversely proportional to A_{sa}. That changes in the second half, where I_z surpasses I_y in value, and therefore $I_y = I_{min}$. In this state of the optimization, that would happen at about when A_{sa} would take on the value of 22 m^2. The term $(I_{max} - I_{min})$ now is $I_x - I_y$, which is proportional to A_{sa}. That means that the optimization of P_{tot} or τ_{tot} would lead A_{sa} to take on the value of 22, as that would minimize the deviation of $(I_{max} - I_{min})$. The overall form of the plots above vary with the change in the values of (almost) all the design variables. The point of intersection between I_y and I_z varies as well. What is special to this case is that along the optimization process, the order of the values of the moments of inertia changes, which results in a varying direction of the values of the design variables. The result is that the value of A_{sa} itself is not the priority when optimizing P_{tot}, but rather the minimization of the divergence of the moments of inertia.

At this point the behavior of the MDO has been introduced. The rest of this section focuses on practical matters of optimization, from initialization to variable updates. In the $MDOuU$ of Chapter 5, the convergence of the three QoIs are thoroughly examined from the analysis' optimal results.

3.2.4 Design Variable Initialization

In gradient-based methods, the initialization plays a critical role in shaping the outcome. Updating the variables with the derivative as a driving factor, there exists the risk of converging to a local optimum instead of the global. This case has to be investigated. The *Latin Hypercube Sampling* (LHS) method [15] is employed to mitigate this issue. LHS is widely used in probabilistic analyses, where the objective is to generate a diverse and well-distributed set of samples while limiting the required sample size. This is achieved by partitioning the domain of each variable into N intervals, with one sample drawn from each interval. The resulting samples are then combined to produce N points in the multidimensional design space, ensuring an efficient coverage of each variable. For the purposes of optimization, it enhances the exploration of the design space and reduces the likelihood of convergence to suboptimal local minima, by providing a well-distributed set of starting points.

3.2.5 Variable Update

Since the minimization problem is solved using SD, the variable correction $\vec{\Delta b}$ is taken in the opposite direction of the objective function gradient. The variable update is then:

$$\vec{b}_{new} = \vec{b}_{old} + \vec{\Delta b} \quad \text{, with} \quad \vec{\Delta b} = -\eta_{SD} \nabla \hat{F}_{\vec{b}}$$

The value of the scalar quantity η is chosen heuristically for optimal convergence. Each objective function requires a different η for stable results. *SD* is the most basic and robust variable update method, but it may lead to slower convergence compared to more advanced correction approaches. In this analysis, its simplistic setup makes it ideal.

3.2.6 Maximum Correction Criterion

If $\vec{\Delta b}$ turns out to be small, the value of η should be increased. That could mean exploding corrections for certain design variables. This is why a criterion of maximum correction is enforced. Each Δb_l term is normalized with the respective variable range of definition. The relative correction is then $\frac{\Delta b_l}{range_l}$. The maximum relative correction $\left.\frac{\Delta b_l}{range_l}\right|_{max}$ is found . If the maximum relative correction is larger than intended, the entire $\vec{\Delta b}$ is scaled as follows:

$$\vec{\Delta b} \rightarrow \frac{\vec{\Delta b}}{\left.\frac{\Delta b_l}{range_l}\right|_{max}} 0.001$$

The result now is that the maximum relative step out of all the variables is up to the designer's choice, in this case being equal to 0.001. This normalization prevents the correction from blowing out of proportion at each iteration.

Chapter 4

Uncertainty Quantification of the FS

This section introduces the UQ framework applied to the FS case. The UQ requires the converged evaluation of the MDA, to use feasible values of all measures, in order to propagate input uncertainties through the system and evaluate their impact on the selected QoIs.

4.1 Identification of the FS Uncertain Variables

The $MDAuU$ baseline case considers nine uncertain input variables, distributed across the different disciplines of the system. These variables represent quantities that are not known with complete precision due to modeling assumptions, environmental variability, and inherent limitations in parameter estimation. As a result, they are treated probabilistically rather than deterministically. The case framework represents uncertain variables through normal distributions. This assumption provides a balance between capturing variability and maintaining a model that remains analytically manageable and physically intuitive.

Although they correspond to similar physical characteristics as the design variables of the previous chapter, their separation is functional: the uncertain variables are provided by the literature-based FS study as stochastic parameters, whereas the design variables are defined in the present work as controllable optimization parameters.

Already it has been discussed how the orbital altitude H is targeted at 18×10^3 km. In reality, the gravitational interaction between bodies that deviate from perfect spherical symmetry results in an orbit that is not perfectly circular, but exhibits variability around this nominal value. This effect is represented here through a standard deviation on the order of 10^3 km, serving as a practical approximation of more complex dynamics that would otherwise require significantly higher modeling fidelity. Along the same lines, normal distributions are assigned to a range of system parameters, including satellite configuration measures affecting attitude properties, and power-related quantities, providing a consistent representation of uncertainty across the model.

Each uncertain variable is thus modeled using a truncated normal distribution, characterized by a mean value μ and a standard deviation σ. The uncertainty bounds are expressed in a 6σ format, providing representative lower and upper limits a and b, respectively. The adopted notation is therefore $[\mu, \sigma, a, b]$:

Orbit Uncertain Variable

H, orbit altitude $[m]$: $[18 \times 10^6, 1 \times 10^6, 15 \times 10^6, 21 \times 10^6]$

Power Uncertain Variable

P_{other}, extra power for bigger margin of safety $[W]$: $[1000, 50, 850, 1150]$

ACS Uncertain Variables

C_d, drag coefficient [-]: $[1, 0.3, 0.1, 1.9]$
L_a, moment arm for aerodynamic torque $[m]$: $[2, 0.4, 0.8, 3.2]$
θ, deviation of moment axis $[deg]$: $[15, 1, 12, 18]$
L_{sp}, moment arm for radiation torque $[m]$: $[2, 0.4, 0.8, 3.2]$
F_s, average solar flux $[Wm^{-2}]$: $[1000, 50, 850, 1150]$
q, reflectance factor [-]: $[0.5, 0.1, 0.2, 0.8]$
R_D, satellite residual dipole $[Am^2]$: $[5, 1, 2, 8]$

Fig. 4.1 illustrates the uncertain input configuration on the MDA. In this thesis, the UQ analysis is performed computationally using the *Method of Moments* (MoM). The computationally expensive but reliable *Monte Carlo* method is also employed as a reference to validate the MoM results.

The Monte Carlo Simulation

The MC simulation demands a large pool of samples of random initializations of the uncertain variables. Then, the statistical moments are computed using the expressions suited for discrete samples,

$$\mu_F = \frac{1}{N}\sum_{i=1}^{N} F_i \quad , \qquad \sigma_F^2 = \frac{1}{N-1}\sum_{i=1}^{N}(F_i - \mu_F)^2 \tag{4.1}$$

where N is the sample size. Total randomness in sample initialization is not an ideal approach for obtaining a diverse and representative sample pool. As has already been established, the LHS ensures improved results. With each initialization, the

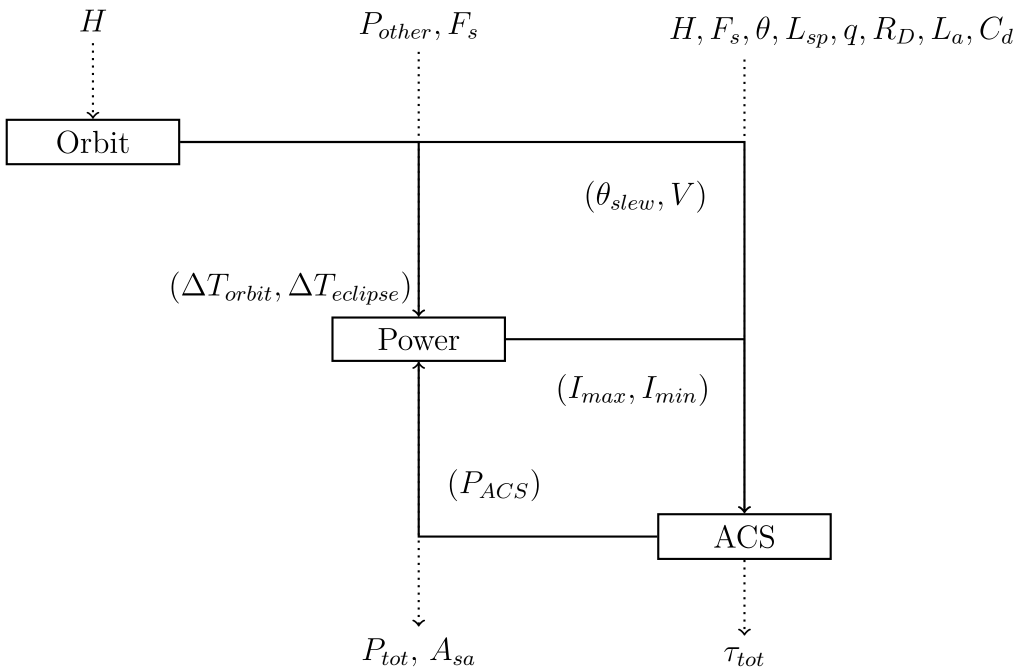

Figure 4.1: Uncertain Inputs and Outputs of the FS system.

MDA is solved to system convergence as dictated by the MDF, and the three QoI values are extracted. The procedure is presented in Algorithm 2.

Algorithm 2 MC Simulation using LHS

```
Set the sample size N
Generate N samples using LHS over the 6σ domain of each uncertain variable
for i = 1 to N do
    Solve the MDA for sample i
    Extract the values of the three QoI
end for
Compute the statistical moments of the QoI
```

The MC method remains computationally expensive, even when combined with LHS. Convergence of the mean is achieved after approximately 1,000 samples, whereas adequate estimation of the standard deviation requires more than 50,000 samples.

4.2 The Method of Moments

It is shown in Appendix B that the statistical moments of each QoI, here denoted by F, are given by:

$$\begin{aligned}\mu_F =& F|_{\bar{c}} + \frac{1}{2}\sum_{i=1}^{M} \left.\frac{d^2F}{dc_i^2}\right|_{\bar{c}} \sigma_i^2 \\ \sigma_F^2 =& \sum_{i=1}^{M}\left[\frac{dF}{dc_i}\right]^2 \sigma_i^2 + \frac{1}{2}\sum_{i=1}^{M}\sum_{j=1}^{M}\left[\frac{d^2F}{dc_i dc_j}\right]^2 \sigma_i^2\sigma_j^2\end{aligned} \tag{4.2}$$

All the derivatives needed were computed analytically in Appendix C. The procedure implemented is thus presented in Algorithm 3:

Algorithm 3 Uncertainty Quantification using the Method of Moments

1: Solve the MDA to convergence
2: Solve the coupled system to obtain the first-order derivatives using DD
3: Solve the coupled system to obtain the second-order derivatives using DD or AM
4: Compute the statistical Moments of the QoI using the MoM

The MoM, although more complex to formulate, requires no costly sampling, as the MDA is converged only once, followed by the DD–DD or DD–AM derivative evaluations. The associated computational cost arises from the derivative calculations and is presented relative to the primal convergence cost in Appendix C.

4.3 UQ Results for the FS

The results of the UQ for the MD system of the FS are listed in Table 4.1, comparing the MoM with the MC simulation, which highlights the high computational accuracy of the second-order derivatives presented in Appendix C.

The UQ analysis of the FS case provides a probabilistic characterization of the system's key design quantities. Although parameters such as the solar array area A_{sa} are ultimately realized as single, deterministic values in the constructed satellite, their computed mean values represent the nominal design targets dictated by the analysis. The associated standard deviations quantify the expected variability around these targets due to the presence of uncertainty in the system inputs, in the

QoI		MoM	MC	divergence(%)
τ_{tot} $[Nm]$	μ	1.17e-02	1.17e-02	-2.57e-03
	σ	4.29e-03	4.3e-03	1.65e-01
P_{tot} $[W]$	μ	1130.08	1130.07	-8.85e-05
	σ	56.24	56.26	3.56e-02
A_{sa} $[m^2]$	μ	11.87	11.87	2.30e-03
	σ	6.2e-01	6.21e-01	9.68e-02

Table 4.1: Statistical Moments comparison, MoM vs MC.

FS case being the orbit conditions. In practical terms, this implies that a solar array sized according to its mean value may, under varying conditions, prove either insufficient or excessive, within bounds described by its standard deviation. This variability is not incidental but intrinsic to the operating environment and modeling assumptions.

It should be noted, however, that the computation of the mean and standard deviation do not provide direct insight into whether the design is more likely to be undersized or oversized. Nevertheless, these measures remain adequate for quantifying the magnitude of uncertainty and the expected spread of the response around its mean.

By explicitly quantifying this uncertainty, the analysis provides guidance for engineering decision-making beyond nominal design, towards employing additional measures to ensure reliable operation. For example, energy storage systems can be incorporated to compensate for fluctuations in power generation, thereby mitigating the effects of adverse orbital conditions. Thus, the goal of the UQ is to indicate not only what the nominal design should be, but also what complementary strategies are required to accommodate variability in real-world operation.

The total disturbance torque acting on the satellite is estimated to have a mean value of the order of $\mathcal{O}(0.01)$ Nm, while the corresponding power requirement is approximately $\mathcal{O}(1)$ kW. These estimates lead to a nominal solar array size of $\mu_{A_{sa}} \simeq 12$ m^2. Accounting for uncertainty, an upper bound for the A_{sa} based on the 3σ criterion is obtained, leading to a conservative estimate of the minimized value::

$$\mu_{A_{sa}} + 3\sigma_{A_{sa}} \simeq 13.7 \text{ m}^2.$$

Adopting this value would correspond to a conservative design choice, potentially resulting in oversizing within the context of the present analysis. Nevertheless, the interval [12, 13.7] m^2 can be interpreted as a reasonable design range, providing a practical estimate of the required solar array size at this preliminary stage, perhaps accompanied by suitable energy storage systems, such as lithium-ion batteries capable of delivering power on the order of 1 kW, to compensate for fluctuations in power generation.

However, since the QoIs are coupled, oversizing the solar array does not necessarily constitute a desirable approach. An increase in panel area leads to higher disturbance torques, which in turn raise the ACS power requirements. As a result, part of the additional power generated by the larger array is effectively offset by the increased total power demand P_{tot}. This highlights the need for a more balanced design approach. A conservative assessment based on a 3σ margin indicates an additional power requirement of approximately $3\sigma_{P_{tot}} \simeq 170$ W. This value can be interpreted as the minimum capacity required from an auxiliary power storage system integrated within the satellite.

Chapter 5

FS Optimization under Uncertainty

The *UQ* formulation has been presented, along with the *MDO* framework. This chapter combines both methods to formulate a robust design for the *QoI*s of the *FS* case. It is therefore crucial to describe why the topic of robustness must be implemented in the design process. To provide an example, the minimization of the mean value of the solar array area A_{sa} leads to a more compact and lightweight design; however, reducing its standard deviation ensures that this requirement is consistently satisfied under uncertain conditions. Similarly, minimizing the mean total power P_{tot} avoids unnecessary oversizing, while controlling its variability guarantees that power demands are reliably met. In the case of the disturbance torque τ_{tot}, reducing its mean value limits the nominal control effort required, whereas minimizing its standard deviation ensures stable and predictable attitude behavior. The optimization process therefore seeks a balance between performance and reliability, where both the expected values and the associated uncertainties of the *QoI*s are taken into account.

5.1 Bi-objective Optimization Turned Single-Objective

The *Weighted Sum* formulation is chosen as a practical means of handling competing objectives, such as performance and robustness, within a single scalar optimization problem. The optimization is performed by selecting one *QoI* at a time, with a weighted sum of its statistical targeted as the global objective function:

$$\hat{F} = k\ \mu_F + (1-k)\sqrt{\sigma_F^2} \quad , \qquad \text{where} \quad k \in [0,1].$$

This way, the bi-objective optimization is solved as multiple single optimization problems, with varying weights k: the trade-off between nominal performance and sensitivity to uncertainty can be explicitly controlled- for extreme values of k ($k \to 1$ and $k \to 0$) the optimization focuses solely on one of the two statistical moments, the mean value or the standard deviation respectively. Such scalarization techniques are widely adopted in MDO, particularly when computational cost or complexity must be limited. However, this reduction introduces certain limitations. A single weighted formulation cannot capture the full spectrum of optimal trade-offs that would be revealed through a true multi-objective analysis. Despite this drawback, the approach remains effective for providing insight into the system behavior and for identifying balanced designs under uncertainty, especially in early-stage or conceptual studies.

Substituting the expressions of the statistical moments from Eqs. 4.2, the derivatives of the objective function become:

$$\frac{d\hat{F}}{db_l} = k\left(\frac{dF}{db_l} + \frac{1}{2}\frac{d^3F}{dc_i^2 db_l}\sigma_i^2\right) + (1-k)\frac{2\frac{dF}{dc_i}\frac{d^2F}{dc_i db_l}\sigma_i^2 + \frac{d^2F}{dc_i dc_j}\frac{d^3F}{dc_i dc_j db_l}\sigma_i^2\sigma_j^2}{2\sqrt{\left[\frac{dF}{dc_i}\right]^2\sigma_i^2 + \frac{1}{2}\left[\frac{d^2F}{dc_i dc_j}\right]^2\sigma_i^2\sigma_j^2}}$$

Therefore, for the purposes of this chapter, there are three additional derivative categories to compute:

1. The derivatives of the QoI with respect to $\vec{b}$: $\dfrac{dF}{db_l}$.
2. The mixed derivatives of the QoI, first with respect to the uncertainties, then with respect to $\vec{b}$, $\dfrac{d^2F}{dc_i db_l}$.
3. The respective third-order mixed derivatives $\dfrac{d^3F}{dc_i^2 db_l}$.

The objective functions' gradients, which are comprised of the gradients of the QoI and those of the statistical moments of the QoI, with respect to $\vec{b}$, are calculated using *Forward Differences*, as any alternative derivative computation method, such as DD or AM, would be exceedingly cumbersome—even from the general expression of the second-order derivatives, 3D matrices surface. This way, for each optimization iteration, both the primal MDA and the UQ will be solved $N+1$ times, each time providing another set of the three derivative terms presented above for the FD.

5.2 Optimization Procedure

Although the FS model defines three distinct QoIs, these outputs are not independent. Instead, they arise from a single coupled physical system and are inherently interrelated through the underlying MD interactions. Their separation reflects different physical perspectives of the same design problem rather than independent performance targets. Specifically, each QoI emphasizes a different aspect of system behavior: energy generation capability (P_{tot}), geometric and structural design requirements (A_{sa}), and attitude stability through disturbance effects (τ_{tot}). While these quantities are tightly coupled, treating them separately enables the identification of how each physical mechanism constrains or drives the overall system response. To assess their correlation and determine their relative prioritization, the first set of optimization runs is conducted as presented in Table 5.1. Algorithm 4 then presents the order of operations for each optimization run (i.e., for a single weight factor k).

Set	**Running for**
1st Set: for $F = \tau_{tot}$	$k_{\text{weight}} = 0$ $k_{\text{weight}} = 1$
2nd Set: for $F = P_{tot}$	$k_{\text{weight}} = 0$ $k_{\text{weight}} = 1$
3rd Set: for $F = A_{sa}$	$k_{\text{weight}} = 0$ $k_{\text{weight}} = 1$

Table 5.1: Initial Optimization Runs.

Algorithm 4 Single-weight k Optimization Procedure using FD

Set convergence tolerance ε
while not converged **do**
  Solve the MDA and UQ for the current design point
  for $d = 1$ to N_d **do**
    Solve the MDA for the forward difference in the d variable
    Solve the UQ for the forward difference in the d variable
  end for
  Compute the FD with respect to the design variables
  Implement *Steepest Descent*
  Implement maximum correction criterion
end while

For convergence to the optimal value, the number of optimization cycles typically reaches the order of several hundred. If the design variables were of a similar nature, sharing comparable physical meaning, scale, and sensitivity, the convergence rate would be significantly faster. However, in this case, the variables belong to substantially different aspects of the analysis, thus the design space can be termed as ill-conditioned. The implementation of the maximum correction criterion also considerately dampens every step update.

5.3 Results

For conclusive results, multiple initializations of the design variables $\vec{b}$ generated by the LHS method are evaluated. In general, the size of the design space would require a sample size on the order of thousands; however, in this case, 100 samples are generated for each QoI optimization. Additionally, for each initialization sample, the vector of the k-weights used consists only of the two extreme values 0 and 1. The objectives are then the standard deviation σ_F for the first run, and the mean value μ_F for the second. The results are presented separately for each QoI-driven optimization run.

5.3.1 Robustness of τ_{tot}

The baseline values of the statistical moments of τ_{tot} are:

$$\mu_{\tau_{tot}} = 0.011 \quad Nm$$

$$\sigma_{\tau_{tot}} = 0.0043 \quad Nm$$

Table 5.2 presents the convergence of the other two QoI when the optimal statistical moments are achieved for τ_{tot}. The results correspond to the LHS initialization that yielded the best performance.

τ_{tot}		A_{sa}	P_{tot}
$\mu_{\tau\_tot} = 0.0076$	μ_{other}	32.81	1107.69
	σ_{other}	1.66	53.17
$\sigma_{\tau\_tot} = 0.0028$	μ_{other}	10.35	1092.39
	σ_{other}	0.52	52.58

Table 5.2: τ_{tot}'s contribution to the other QoIs.

It is evident that while the QoI P_{tot} converges in a satisfying set of values, the QoI A_{sa} does not benefit from this approach. The search continues for the other QoI.

5.3.2 Robustness of P_{tot}

The baseline values of the statistical moments of P_{tot} are:

$$\mu_{P_{tot}} = 1130.08 \quad W$$

$$\sigma_{P_{tot}} = 56.26 \quad W$$

As before, Table 5.3 is drawn:

P_{tot}		A_{sa}	τ_{tot}
$\mu_{P\_tot} = 1089.74$	μ_{other}	18.09	0.0075
	σ_{other}	0.91	0.0028
$\sigma_{P\_tot} = 52.30$	μ_{other}	13.99	0.0076
	σ_{other}	0.71	0.0027

Table 5.3: P_{tot}'s contribution to the other QoIs.

It is evident that the QoIs of P_{tot} and τ_{tot} are strongly linked in their convergence, while the A_{sa} is not optimized ideally once more.

5.3.3 Robustness of A_{sa}

The baseline values of the statistical moments of A_{sa} are:

$$\mu_{A_{sa}} = 11.87 \quad m^2$$

$$\sigma_{A_{sa}} = 0.62 \quad m^2$$

Table 5.4 shows that minimization of A_{sa}'s statistical moments also offers optimal results for the other two QoI's moments.

A_{sa}		$Ptot$	τ_{tot}
$\mu_{A\_sa} = 9.26$	μ_{other}	1089.77	0.0075
	σ_{other}	52.3	0.0028
$\sigma_{A\_sa} = 0.47$	μ_{other}	1089.77	0.0076
	σ_{other}	52.29	0.0028

Table 5.4: A_{sa}'s contribution to the other QoIs.

This makes it clear that for the remainder of the analysis, the QoI of A_{sa} can safely be targeted as the objective function, for the sake of the collective system robustness.

5.4 Final Set of Runs

The next set of optimization runs uses the initial design space sample that yielded the optimal results for the statistical moments of A_{sa}. In this stage, the weighting parameter k_{weight} is explored over the full range between 0 and 1, instead of only at the boundary values.

Conflicting Directions in Weighted-Sum Objective

It is crucial that the ratio of the two derivatives is taken into account:

$$ratio = \frac{d\sigma_f}{d\mu_f} = \mathcal{O}(0.01)$$

For each QoI, and generally for every variable, this ratio is typically of the order of 10^{-2}. It indicates how small the weighting factor k must be for the term $(1-k)d\sigma_f$ to be substantially larger than $kd\mu_f$; that is, how much $d\mu_f$ needs to be de-emphasized for the derivative of $d\sigma_f$ to factor in the optimization. In this case, the resulting distribution of k values across the various optimization runs is typically skewed toward values below 0.5. However, since the ratio $\frac{d\sigma_f}{d\mu_f}$ is not of steady magnitude order $\mathcal{O}$ throughout the optimization procedure, for the analysis to be conclusive, the vector $\vec{k}$ is finally constructed symmetric around 0.5.

The point of divergence between the various cases of different k-weight values, is when the ratio $\frac{d\sigma_f}{d\mu_f}$ is **negative**. When the ratio is **positive**, the two objectives have the same direction for the given design variable, which means that in the next optimization iteration, both the mean value and that of the standard deviation of said QoI will be decreased. What changes is the magnitude of the increment induced to the next step method. When the ratio is **negative**, the minimization objectives for the mean value and for the standard deviation are contradictory. For every change in the design variable, one objective is increased while the other is decreased. It is concluded heuristically that in the FS case, the ratio is positive more often than not, when the runs converge.

A Pareto front can finally be drawn for the competing values of the statistical moments of the A_{sa}, and is presented in Fig. 5.1. Table 5.5 translates the resulting improved design.

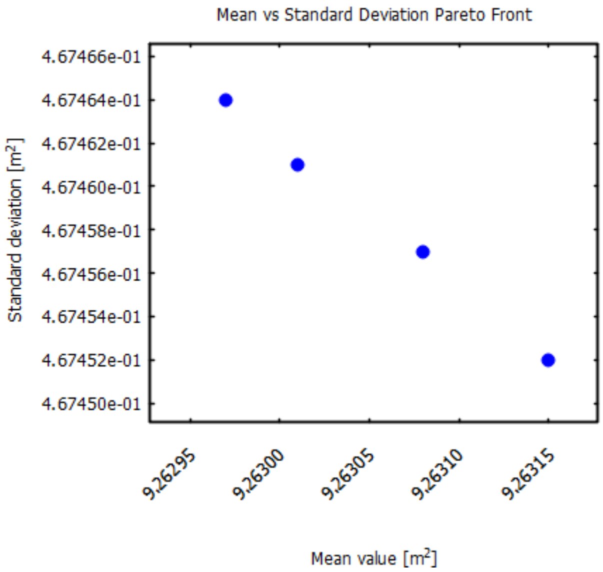

Figure 5.1: Pareto front for A_{sa}.

Metric	Initial Value	Optimized Range	Improvement (%)
$\mu_{A_{sa}}$ $[m^2]$	11.87	9.262 – 9.263	21.962 – 21.963
$\sigma_{A_{sa}}$ $[m^2]$	0.62	0.46745 – 0.46746	24.603 – 24.604

Table 5.5: A_{sa}'s Pareto Optimization Results

Qualitative Results Analysis

The procedure for constructing the Pareto front has a solid mathematical foundation; however, the FS case itself is not ideal for demonstrating such results. Fig. 5.1 presents that the Pareto front loses its multi-objective character, as the deviations between the two objectives are practically negligible in real-world application. This front degeneration cannot be resolved by widening the ranges of the design variables used: it seems that the FS framework exhibits a tight correlation of the first two statistical moments of the QoI.

Similarly, as expected, with the converged results of A_{sa}, the other two QoI indeed converge optimally as well, as shown in the Pareto fronts of τ_{tot} (Fig. 5.2) and of P_{tot} (Fig. 5.3).

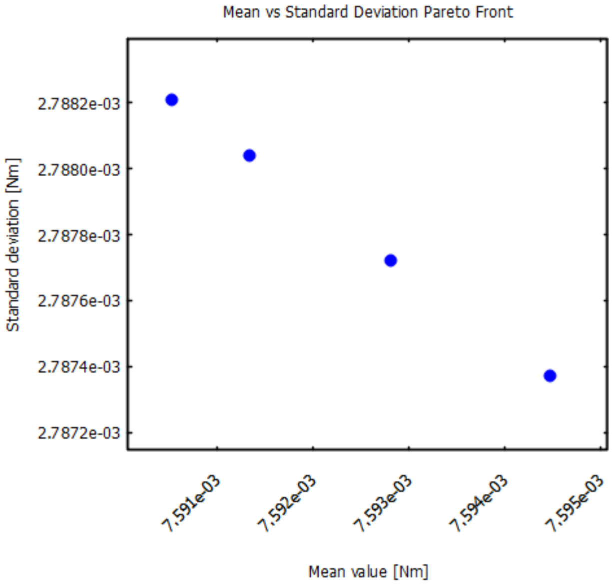

Figure 5.2: Pareto front for τ_{tot}.

τ_{tot} Pareto Optimization Results			
Metric	Initial Value	Optimized Range	Improvement (%)
$\mu_{\tau_{tot}}$ $[m^2]$	1.17e-02	7.59e-03 – 7.594-03	35.1236 – 35.1235
$\sigma_{\tau_{tot}}$ $[m^2]$	4.29e-03	2.787e-03 – 2.788e-03	35.03 – 35.01

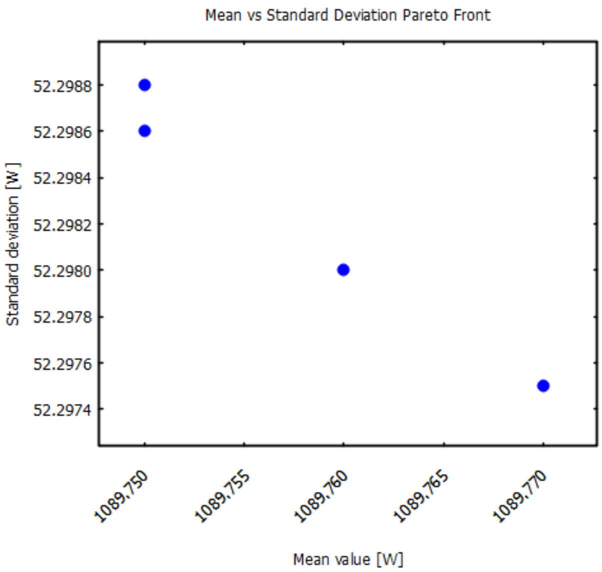

Figure 5.3: Pareto front for P_{tot}.

The only noted difference is that the Pareto front of the P_{tot} (Fig. 5.3) degenerates

P_{tot} Pareto Optimization Results			
Metric	Initial Value	Optimized Range	Improvement (%)
$\mu_{P_{tot}}$ $[m^2]$	1130.08	1089.75 – 1089.77	3.568 – 3.567
$\sigma_{P_{tot}}$ $[m^2]$	56.26	52.297 – 52.298	7.044 – 7.042

even further, to a three-dominant-point diagram.

Pareto Front Assessment

In conclusion, while the Pareto-based formulation is mathematically consistent and fully applicable, its expressive power is limited in the context of the present FS case. The observed near-degeneracy of the Pareto fronts indicates that within the FS framework, instead of independent sources of conflict in the design process, robustness and performance are practically achieved in parallel.

Overall Optimization Conclusions

A final note to the present analysis is that the results obtained in this work should be interpreted primarily as indicators of system behavior rather than definitive quantitative design prescriptions. This study serves as a preliminary investigation into the behavior of the FS framework under uncertainty and optimization. The results should be viewed purely from their conceptual meaning, rather than as direct engineering recommendations.

Chapter 6

Conclusions

The FS framework was extensively examined in order to highlight key aspects across the different disciplines.

The MD case was addressed using multiple approaches for the evaluation of the QoI derivatives, namely the analytical DD–AM formulation for the MoM, as well as an FD approach for the sensitivity derivatives used within the optimization formulation. The system is treated similarly to a single-discipline problem, where the coupled variables are considered state variables governed by the residual form of the governing equations.

The implementation of the AM does not eliminate computational cost, as it relies on the exact same underlying derivative information as the DD method. Its advantage lies in shifting the computational scaling to depend on the number of QoIs ($N_F = 3$), rather than on the number of uncertain variables ($M = 9$). First-order derivatives are evaluated using DD, since the sensitivities $\frac{d\vec{Y}}{d\vec{c}}$ repeatedly surface in the construction of second-order derivatives. As a result, the most cost-effective strategy for second-order derivative evaluation is the DD–AM approach.

The construction of the MoM is not trivial, but it significantly reduces the computational cost associated with estimating statistical moments. In the present case, considering $M = 9$ uncertain input variables, the cost remains below 40 times the MDA convergence time (C.34). In contrast, stochastic approaches such as MC simulation, or quadrature-based methods such as Gauss quadrature, require several thousand samples per optimization iteration to achieve comparable accuracy for up to the second statistical moment σ_F^2.

The MDO follows the monolithic MDF approach, in which the system is fully converged at each cycle before computing derivatives of a single, system-level, objective function. Although the three QoIs are inherently coupled, cases were performed where each QoI was individually prioritized for the first set of runs. The results show that the A_{sa}-driven optimization consistently yields satisfactory performance across the remaining two QoIs.

The Weighted Sum method was employed to express the competing robustness objectives of the two statistical moments of each QoI into a single objective function per optimization run. To mitigate convergence to local optima, LHS was employed for the initialization of the design space, ensuring a sufficiently diverse set of starting points, for sufficiently large experimentating runs. In addition, the design update strategy was carefully controlled: although steepest descent employs a constant step size η, the magnitude of the update vector is limited to keep the design variable updates within sensible bounds. While this makes convergence more restricted, it is essential for numerical stability.

Finally, a Pareto front is generated over a broad range of weighting factors k_{weight}. Although the resulting front does not provide practically sharp robustness–optimality trade-offs, it nevertheless offers insight into the strong coupling between competing objectives in the FS case. The optimization reduces the mean and standard deviation of A_{sa} by 22% and 24%, respectively. The corresponding reductions for P_{tot} are 3.5% and 7%, while both the mean and standard deviation of τ_{tot} are reduced by 35%.

Future work may include the extension of the framework to non-Gaussian uncertainty models and non-symmetric probability distributions. Additionally, the employment of the Epsilon-Constraint method for the Pareto front formulation can provide even richer results, as, unlike Weighted Sum approaches, it is capable of capturing non-convex regions of the Pareto front, thereby revealing solutions that might otherwise remain undiscovered.

Appendix A

Fire Satellite Equation System

The FS system of equations is presented to illustrate the underlying physics of the case. General forms of the equations are described, and Table A.1 provides the deterministic values that define the system. The equations are described by order of disciplines, in order to show the entire formulation of the system dependencies.

A.1 Orbit Equations

As established, the translational motion of the satellite is governed entirely by the Earth's gravitational attraction. The gravitational force binding the Earth-satellite system, as was presented by Isaac Newton in his work on the universal law of gravitation [11], is:

$$F_{gravitational} = \frac{GM_{earth}m_{sat}}{(R_{earth} + H)^2} \tag{A.1}$$

where $(R_{earth} + H)$ is the orbit distance from the center of the Earth and G the universal gravitational constant. The product GM_{earth} is Earth's gravity constant. Due to the large mass difference between the Earth and the satellite, the system's complex elliptical action–reaction trajectory reduces to a simple uniform circular orbit. The Earth is practically fixed in place, and the satellite travels around it at a constant altitude. For that to happen, the gravitational force acts as a *centripetal* force on the satellite, as such is the only way that results in circular motion ($F_{gravitational} = F_{centripetal}$).

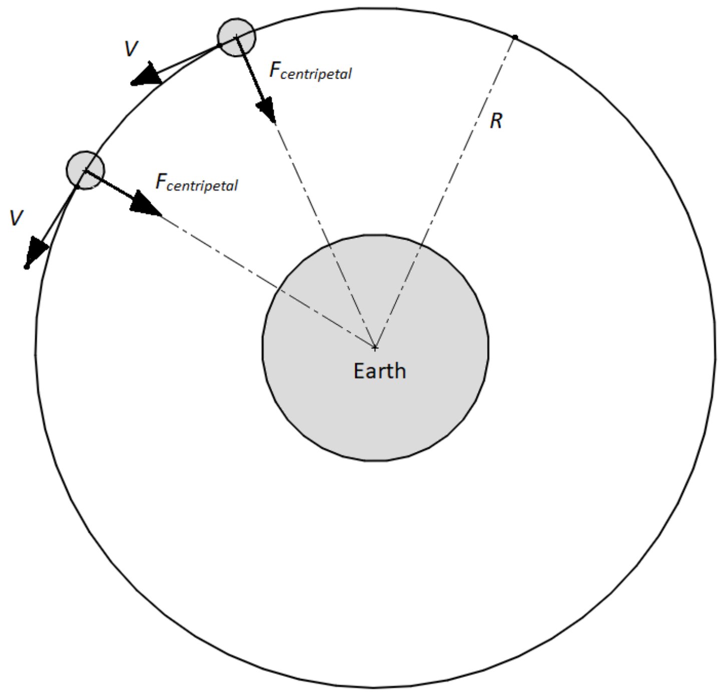

Figure A.1: Centripetal Force causing Orbit

The velocity of the flying object is always tangent to the circular orbit track. The vector of the force $\vec{F}_{centripetal}$ binding the satellite in its orbit is always perpendicular to its velocity vector $\vec{V}$. If the magnitude of the velocity meets a certain value, the result of this always-perpendicular force is the constantly changing velocity direction, with no change in its magnitude. The centripetal acceleration $\vec{a}_{centripetal}$ changes only the direction of the velocity, not its magnitude. The expression of a centripetal force is:

$$F_{centripetal} = ma_{centripetal} = m\frac{V^2}{R}$$

where m is the mass of the object performing the circular trajectory, V is its velocity, and R is the distance of the center of mass of the object from the axis of revolution. In this case, R is the distance between the centers of mass of the two bodies. Eq. A.2 adapts the general force to the satellite case

$$F_{centripetal} = m_{sat}\frac{V^2}{(R_{earth} + H)} \tag{A.2}$$

Setting Eqs. A.1 and A.2 equal to each other and solving for the satellite orbit velocity, the first orbit equation is acquired:

$$V = \sqrt{\frac{GM_{earth}}{R_{earth} + H}} \tag{A.3}$$

This is the velocity magnitude needed to stay in orbit at the desired altitude H. The velocity is inversely proportional to the square root of the bodies' distance. The bigger the altitude H, the slower the satellite traverses through space, the bigger its orbit period.

It is crucial to know how much time is spent illuminated by the Sun, and how much time is spent behind Earth's shadow. Since the satellite velocity is constant, the orbit period can be calculated corresponding to the time needed for the satellite to cover the orbit circumference of $2\pi(R_{earth} + H)$, hence given by :

$$\Delta T_{orbit} = \frac{2\pi(R_{earth} + H)}{V} = 2\pi\sqrt{\frac{(R_{earth} + H)^3}{GM_{earth}}} \quad \text{(using } V \text{ from Eq. A.3)} \tag{A.4}$$

The satellite altitude H also determines the duration spent within the Earth's shadow. Given the large Sun–Earth distance, the Earth's shadow is approximated as a cylinder extending from the planet, rather than a conical shape. Fig. A.2 shows how the length of the eclipse part of the satellite's journey is calculated.

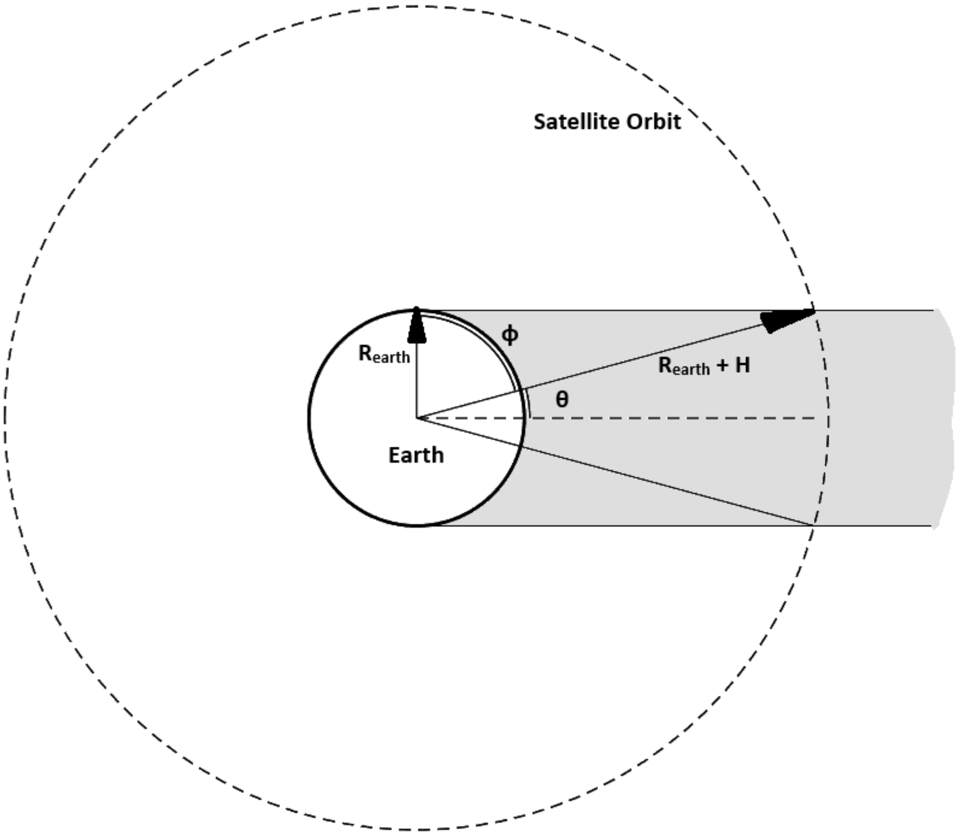

Figure A.2: Angle of orbit eclipse

The angle subtended by the eclipse arc is 2θ, and since the central angles θ and ϕ are complementary,

$$sin\theta = cos\phi = \frac{R_{earth}}{R_{earth} + H} \tag{A.5}$$

The eclipse arc is equal to:

$$\Delta S_{eclipse} = 2\theta(R_{earth} + H) = 2(R_{earth} + H) \arcsin\left(\frac{R_{earth}}{R_{earth} + H}\right) \tag{A.6}$$

Knowing that the satellite velocity is constant, the time spent in the eclipse arc is:

$$\Delta T_{eclipse} = \frac{\Delta S_{eclipse}}{V} = \frac{2(R_{earth} + H)}{V} \arcsin\left(\frac{R_{earth}}{R_{earth} + H}\right) \tag{A.7}$$

Substituting V from Eq. A.4:

$$\Delta T_{eclipse} = \frac{\Delta T_{orbit}}{\pi} \arcsin\left(\frac{R_{earth}}{R_{earth} + H}\right) \tag{A.8}$$

The last aspect governed by the orbital state, is the field of view of the satellite. This aspect is solved for in this discipline, to be used in the third one, of the ACS. Based on the satellite's monitoring capabilities, the target diameter $\varnothing_{target}$ is a given input of the case. With this measure, along with the satellite orbit altitude H, the scope's field-of-view angle is defined. For the ACS analysis, the system requires a target angle for slewing, whose role will be discussed in the following section. The target slewing angle θ_{slew} is defined by the case as the half-angle of the scope's field-of-view angle. Fig. A.3 illustrates the geometry examined.

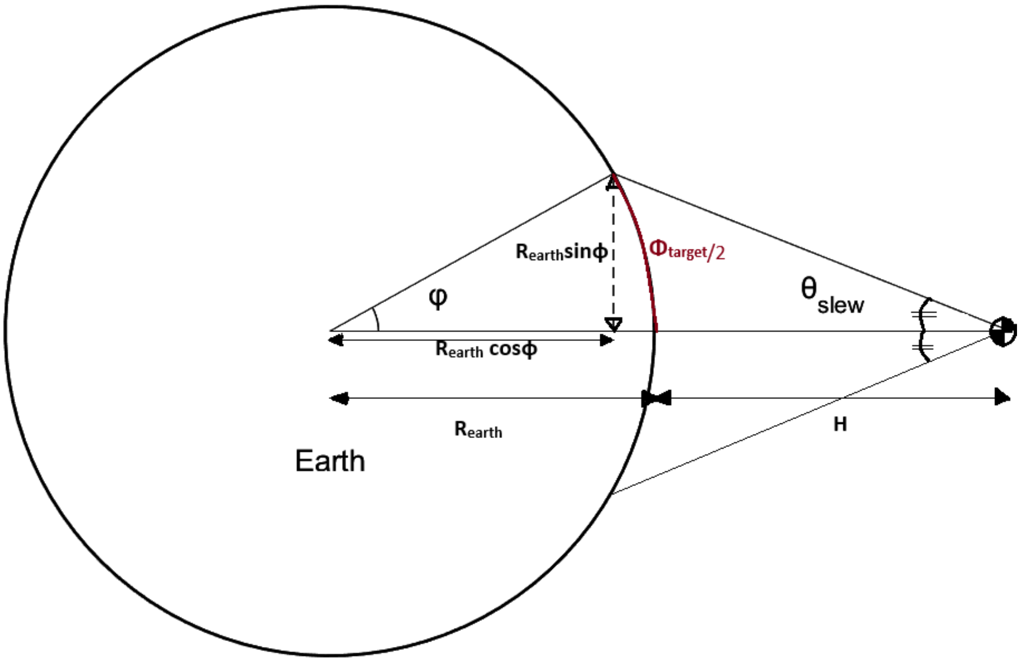

Figure A.3: Angle of observation θ_{slew}

This depiction is greatly exaggerated. The target diameter $\varnothing_{target}$ amounts to 0.59% of the circumference of the Earth (its exact value is listed in Table A.1). Fig. A.3 illustrates that because of the curvature of the Earth, the area of observation does not lie on a plane, but on a spherical section (a circle arc in the two-dimensional figure). To proceed with the calculations, the resulting triangular geometry is examined. The right triangle that θ_{slew} belongs to, is formed by two vertical sides, one of size $R_{earth}sin\phi$ and one of size $(R_{earth} + H - R_{earth}cos\phi) = (R_{earth}\,(1 - \cos\phi) + H)$. That gives:

$$\tan\left(\theta_{slew}\right) = \frac{R_{earth}\sin\phi}{R_{earth}\left(1-\cos\phi\right)+H} \quad \Rightarrow \quad \theta_{slew} = \arctan\left(\frac{\sin\phi}{1-\cos\phi+\frac{H}{R_{earth}}}\right) \tag{A.9}$$

where the central angle ϕ is:

$$\phi = \frac{Arc}{Radius} = \frac{\varnothing_{target}}{2R_{Earth}} \tag{A.10}$$

A.2 Attitude Control System

Although the *ACS* constitutes the third discipline of the system, it is presented before the *Power* discipline to improve the coherence of the formulation, as it defines the disturbance torques that the power subsystem must ultimately compensate for.

The *ACS* governs the rotational motion of the satellite by addressing the torques generated by forces that do not act directly through its center of mass. These disturbance torques arise from multiple sources, including gravitational effects, whose contribution to the translational motion of the satellite has already been discussed. The remaining forces are considered only in terms of their contribution to torque generation, rather than their effect on the satellite's translational motion, as the *FS* analysis does not address long-term orbital conditions and their translational effects are therefore considered negligible.

Slewing Torque

This represents the maximum torque the *ACS* must generate to slew the satellite, either to point its sensor toward a new target or to orient its panels toward the Sun. The reference angle for this maneuver, $2\theta_{slew}$, that is achieved under a constant angular acceleration a_γ over a duration Δt_{slew}, is equal to:

$$2\theta_{slew} = \frac{1}{2}a_\gamma \Delta t_{slew}^2 \quad \Rightarrow \quad a_\gamma = \frac{4\theta_{slew}}{\Delta t_{slew}^2} \tag{A.11}$$

Multiplying with the moment of inertia, the torque needed for the angle displacement is obtained. Taking the most demanding scenario power-wise, the rotation must be around the axis that has the maximum moment of inertia (I_{max}), whichever it is. Thus,

$$\tau_{slew} = I_{max}\frac{4\theta_{slew}}{\Delta t_{slew}^2} \tag{A.12}$$

Gravity Gradient Torque

It has already been established that the main force acted on the satellite is the gravitational pull of the Earth. According to Eq. A.1, that force is inversely proportional to the square of the distance between the center of the Earth, and the body of the satellite. The satellite is not spherical. That means that there is also a torque acted upon its body. Fig. A.4 helps visualize the analysis:

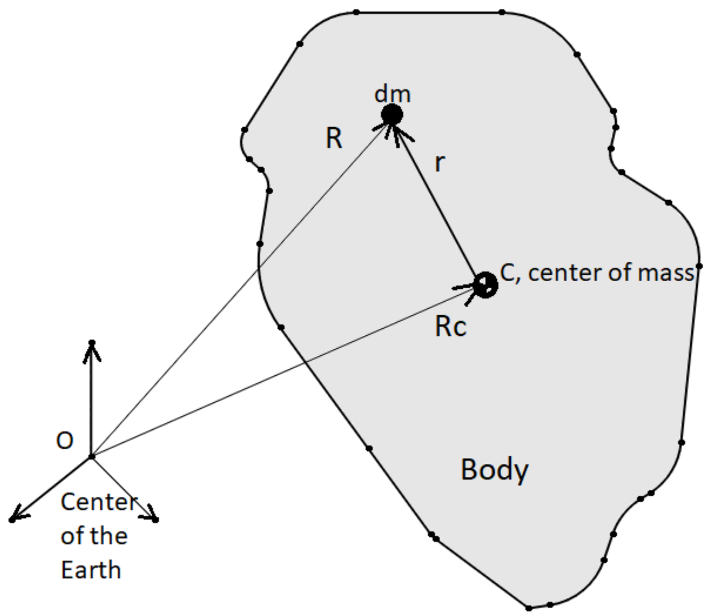

Figure A.4: The gravity gradient analysis

The element dm of Fig. A.4 is attracted to the center of the Earth as shown in Eq. A.1. At this stage vectors are needed because the body is discretized and the expressions of the relative distances within the satellite are necessary. The gravitational force acted on each element is already presented to be:

$$dF_g = GM_{earth}\frac{dm}{R^2}, \quad \text{along the unit vector:} \quad d\hat{F}_g = -\frac{\vec{R}}{|\vec{R}|} \ .$$

Every infinitesimal force dF_g generates a torque (and therefore an angular acceleration) around the satellite center of mass, which, by definition, equals to:

$$d\vec{\tau_g} = \vec{r} \times d\vec{F}_g,$$

where r is the distance between the center of mass and the respective element dm.

Substituting $\vec{R}$ as $\vec{R}_c + \vec{r}$ and integrating the torques throughout the entire body, the gravity gradient torque is computed:

$$\vec{\tau_g} \quad = \quad \int_{\text{Body}} \vec{r} \times d\vec{F}_g \quad = \quad - \int_{\text{B}} \vec{r} \times GM_{earth} \frac{(\vec{R}_c + \vec{r})}{R^3} dm$$

Skipping the calculation of the integral, the gravity gradient torque is finally a vector defined as:

$$\vec{\tau_g} = \frac{3GM_{earth}}{R^3} \vec{R} \times \left(\mathbf{I} \cdot \vec{R} \right)$$

where $\mathbf{I}$ is the moment of inertia tensor measured in kgm^2. Writing the above equation in the primary axis system:

$$\tau_{g,x} = \frac{3GM_{earth}}{2R^3} \left(I_z - I_y \right) \sin 2\theta$$

$$\tau_{g,y} = \frac{3GM_{earth}}{2R^3} \left(I_x - I_z \right) \sin 2\theta$$

$$\tau_{g,z} = \frac{3GM_{earth}}{2R^3} \left(I_y - I_x \right) \sin 2\theta$$

where θ is the angular deviation of the satellite principal axis and the zenith line, Earth's radial direction. The gravity gradient tends to align the satellite's longest axis to the Earth's radial direction. Recalling that $R = R_{earth} + H$, the torque needed is finally:

$$\tau_{g,max} = \frac{3GM_{earth}}{2 \left(R_{earth} + H \right)^3} \left(I_{max} - I_{min} \right) \sin 2\theta \tag{A.13}$$

no matter the x, y, z coefficient it belongs to.

Aerodynamic Torque

The drag force is exerted by the surrounding air (or, in this case, the sparse atmospheric particles), and is always opposite to the orbit velocity V.

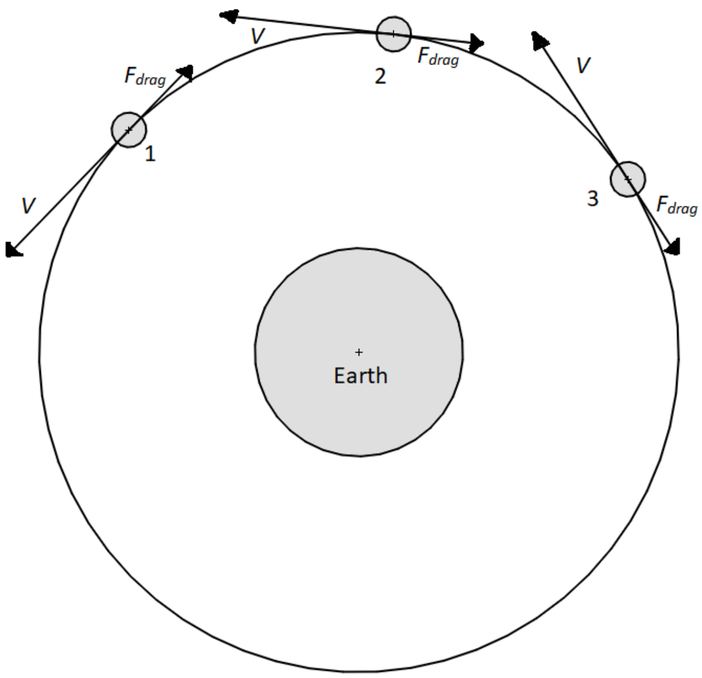

Figure A.5: The drag force

The drag coefficient C_d measures how strong the drag force is compared to the air's dynamic pressure, which consists of the air's density ρ, the satellite surface area A, and the satellite Velocity V:

$$C_d = \frac{F_{drag}}{\frac{1}{2}\rho A V^2}$$

The infinitesimal value of ρ is countered with the square of V, resulting in a drag force that must be accounted for. Assuming a steady C_d for a given satellite geometry (something of great importance in aerospace engineering), the drag force is approximated by the value:

$$F_{drag} = \frac{1}{2} C_d \rho A V^2 \tag{A.14}$$

with the resulting torque being:

$$\vec{\tau}_{drag} = \vec{L}_a \times \vec{F}_{drag}$$

The moment arm L_a is the distance between the satellite center of mass and the net drag force. Substituting from Eq. A.14 results in:

$$\tau_{drag} = \frac{1}{2} L_a C_d \rho A V^2 \tag{A.15}$$

Solar Radiation Torque

This torque arises from the satellite's interaction with the Sun's electromagnetic radiation. Sunlight striking the satellite's surface exerts a small mechanical force through photon impact, which, depending on the satellite's position, may accelerate, or decelerate its translational motion (something that is considered negligible in the scope of this thesis), and tend to turn its body in a constantly changing direction-as shown in Fig. A.6.

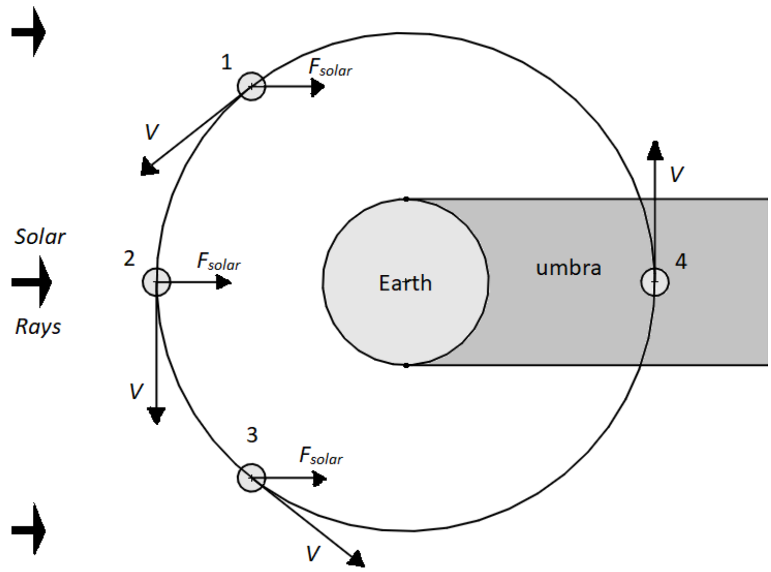

Figure A.6: The solar radiation force

The solar radiation force is expressed as:

$$F_{solar} = \frac{F_s}{c} A_s (1 - q) \cos^2 i$$

where F_s is the average solar flux measured in Wm^{-2}, q is the reflectance factor of the panels, c is the speed of light, A_s is the area reflecting radiation and finally i is the angle between the panels' normal vector and the solar rays. The torque is then:

$$\tau_{sp} = L_{sp} \frac{F_s}{c} A_s (1 - q) \cos^2 i \tag{A.16}$$

Let it be noted that the two torques discussed above use different surface areas of the satellite: A for τ_{drag} and A_s for τ_{solar}. Due to the differing directions of the respective applied forces, these areas are not identical.

Magnetic Field Interaction Torque

The satellite is composed of metal parts, which, over long exposure in the Earth's magnetic field, can get magnetized to an alarming point. If left unchecked, the satellite will align with the magnetic lines of the Earth and will be rendered unable to escape their direction. This torque is equal to:

$$\tau_m = \frac{\mu_0}{4\pi} \frac{2MR_D}{\left(R_{earth} + H\right)^3} \tag{A.17}$$

where M is the Earth's magnetic dipole moment and R_D is the satellite residual dipole, both measured in $\mathrm{A\,m^2}$. The constant μ_0 denotes the permeability of free space, measured in $\mathrm{N\,A^{-2}}$.

Total Torque

The geometric sum of all the disturbing torques above is defined as:

$$\tau_{dist} = \sqrt{\tau_{drag}^2 + \tau_g^2 + \tau_{sp}^2 + \tau_m^2} \tag{A.18}$$

τ_{dist} represents the magnitude of the torque needed to be generated by the ACS to counter all the disturbances in orbit. τ_{slew} represents the maximum required slewing torque generated by the ACS.

For the power analysis that follows, the key point is which of the two torques discussed above has the larger magnitude. The power requirement is then based on this higher value. This hierarchy can change depending on the satellite's orbital state. For the remainder of the analysis, the larger torque is denoted as τ_{tot}:

$$\tau_{tot} = \max(\tau_{slew}, \tau_{dist}) \tag{A.19}$$

The satellite must at all times be capable of producing this total torque (through the use of the three reaction wheels) with the power that is generated from its solar panels.

A.3 Power Analysis

This analysis section focuses on the way the satellite produces power. For this model, the only power consumption is through the use of the three reaction wheels, which set the attitude of the satellite. The power produced from the solar panels must be such that the system works in equilibrium. Once the total torque required to control the satellite has been determined from the ACS discipline, the corresponding attitude control power P_{ACS} can be calculated:

$$P_{ACS} = \tau_{tot}\omega_{max} + 3P_{hold} \tag{A.20}$$

The product $\tau_{tot}\omega_{max}$ is the maximum power the reaction wheels could demand. Each reaction wheel also stores power (P_{hold}) as a fail-safe in case something goes wrong. The total power the satellite has for consumption is:

$$P_{tot} = P_{ACS} + P_{other} \tag{A.21}$$

with P_{other} being an additional margin of safety beyond the required ACS power. The power needed to be generated from the solar arrays, P_{sa} is calculated with respect to the desired $Ptot$:

$$P_{sa} = P_{tot}\frac{\frac{\Delta T_{eclipse}}{0.6} + \frac{T_{sunlight}}{0.8}}{T_{sunlight}} \tag{A.22}$$

where $T_{sunlight}$ is the time per orbit spent facing the sun:

$$T_{sunlight} = \Delta T_{orbit} - \Delta T_{eclipse} \tag{A.23}$$

Psa is acquired from the product of the power production capability (measured in Wm^{-2}) of the solar arrays, and their surface, as follows:

$$P_{sa} = A_{sa}P_{cap} \tag{A.24}$$

The power production capability P_{cap} at the satellite beginning of life (BOL) is

$$P_{BOL} = \eta F_s I_d \cos i \tag{A.25}$$

where η is the array power efficiency, F_s the average solar flux Wm^{-2}, I_d the array inherent degradation and i the sun incidence angle. A conservative, end-of-life power production capability—accounting for long-term degradation—is used in determining A_{sa}. The end-of-life (EOL) production capability is computed as:

$$P_{EOL} = P_{BOL}(1 - \epsilon_{deg})^{LT} \tag{A.26}$$

where ϵ_{deg} is the yearly degradation of array efficiency and LT the lifetime of the satellite. Substituting P_{EOL} as the power production capability in Eq. A.24, the array size is computed:

$$A_{sa} = \frac{P_{sa}}{P_{EOL}} \tag{A.27}$$

At this point, the length L and the width W of the solar array can be defined, based on the length-to-width ratio r_{lw}:

$$L = \sqrt{\frac{A_{sa} r_{tw}}{n_{sa}}} \qquad , \qquad W = \sqrt{\frac{A_{sa}}{r_{tw} n_{sa}}} \tag{A.28}$$

where n_{sa} is the number of the solar arrays, here two. The mass of the array is then calculated as:

$$m_{sa} = 2\rho_{sa} LWt \tag{A.29}$$

where ρ_{sa} the density of the solar array and t its thickness. The moments of inertia of the solar arrays can now be calculated for the local coordinate system x, y, z.

$$\begin{aligned}
I_{sa,X} =& m_{sa} \left(\frac{1}{12} \left(L^2 + t^2 \right) + \left(D + \frac{L}{2} \right)^2 \right) \\
I_{sa,Y} =& m_{sa} \frac{1}{12} \left(t^2 + W^2 \right) \\
I_{sa,Z} =& m_{sa} \left(\frac{1}{12} \left(L^2 + W^2 \right) + \left(D + \frac{L}{2} \right)^2 \right)
\end{aligned} \tag{A.30}$$

These equations describe the computation of the moments of inertia of a rectangular body, including the translation of the inertia tensor according to Steiner's theorem. The total moment of inertia for each axis is the sum:

$$I_{total,i} = I_{sa,i} + I_{body,i} \tag{A.31}$$

for $i = x, y, z$. The satellite body's moments of inertia are also listed in table A.1.

Here ends the power analysis, by calculating the dimensions of the solar arrays needed to produce the necessary power, for the ACS discipline to use.

Follows the list of all the deterministic values used in the original fire satellite case, presented by order of use in the MDA.

Table A.1: Deterministic parameters of the Fire Satellite case by discipline.

Discipline	Symbol	Description	Value
Orbit	R_{earth}	Earth radius [m]	6,378,140
	H	orbit altitude [m]	18×10^{6}
	GM_{earth}	Earth gravitational constant [$\mathrm{m^3\,s^{-2}}$]	3.986×10^{14}
	$\varnothing_{target}$	target diameter [m]	235,000
Power	ω_{max}	reaction wheel max speed [RPM]	6000
	P_{hold}	holding power [W]	20
	P_{other}	extra power margin [W]	1000
	ϵ_{deg}	degradation in power production [$\%\,\mathrm{year^{-1}}$]	0.0375
	LT	spacecraft lifetime [years]	15
	η	power efficiency [-]	0.22
	I_d	inherent degradation of array [-]	0.77
	i	sun incidence angle [°]	0
	r_{lw}	length-to-width ratio of solar array [-]	3
	n_{sa}	number of solar arrays [-]	3
	ρ_{sa}	average mass density [$\mathrm{kg\,m^{-3}}$]	700
	D	distance between panels [m]	2
	t	thickness of solar panels [m]	0.005
	I_{bodyX}	body inertia X axis [$\mathrm{kg\,m^2}$]	6,200
	I_{bodyY}	body inertia Y axis [$\mathrm{kg\,m^2}$]	6,200
	I_{bodyZ}	body inertia Z axis [$\mathrm{kg\,m^2}$]	4,700
ACS	$\Delta_{\tau_{slew}}$	slewing time period [s]	760
	θ	deviation of moment axis [°]	15
	L_{sp}	moment arm for radiation torque [m]	2
	F_s	average solar flux [$\mathrm{W\,m^{-2}}$]	1000
	c	speed of light [$\mathrm{m\,s^{-1}}$]	2.9979×10^{8}
	A_s	area reflecting radiation [$\mathrm{m^2}$]	13.85
	q	reflectance factor [-]	0.5
	M	Earth's magnetic moment [$\mathrm{A\,m^2}$]	7.96×10^{15}
	R_D	satellite residual dipole [$\mathrm{A\,m^2}$]	5
	μ_0	permeability of free space [$\mathrm{N\,A^{-2}}$]	$4\pi \times 10^{-7}$
	ρ	atmospheric density [$\mathrm{kg\,m^{-3}}$]	5.1480×10^{-11}
	A	cross-sectional area in flight direction [$\mathrm{m^2}$]	13.85
	C_d	drag coefficient [-]	1
	L_a	moment arm for aerodynamic torque [m]	2

Appendix B

Statistics Mathematics - Method of Moments

The Method of Moments formulations presented in this appendix are adopted from [10]. The method enables the computation of the statistical moments of the output functions F using only a single converged state of the primal system.

B.1 Statistical Moments Definition

The first statistical moment is the *expected* value, the mean value of the sample. That is acquired by averaging the function F through the probability density function (PDF) $p(c)$:

$$\mu_F = \int F(c)p(c)dc \tag{B.1}$$

For the case of the uncertainty space $\mathbf{c}$ of size M, the integral is equal to:

$$\mu_F = \int_{c_1} \int_{c_1} \cdots \int_{c_M} F(\mathbf{c})p(c_1)p(c_2)\dots p(c_M)dc_1dc_2\dots dc_M \tag{B.2}$$

since the uncertain variables are independent to each other.

The second statistical moment, the variance, is obtained by averaging the square of the same function around the mean value:

$$\sigma_F^2 = \int (F(c) - \mu_F)^2 p(c) dc \tag{B.3}$$

The third and fourth statistical moments, the skewness and kurtosis respectively, are similarly defined as:

$$\gamma_F = \int (F(c) - \mu_F)^3 p(c) dc$$

$$k_F = \int (F(c) - \mu_F)^4 p(c) dc$$

The skewness is null for a symmetric PDF, while the kurtosis takes on the value of $3\sigma^2$ for normal distributions [16].

By definition, the integral of the PDF is equal to:

$$\int p(c) dc = 1 \tag{B.4}$$

What is now needed is an expression of the function F in a way that can be managed in the integrals above. For this purpose, the second-order Taylor expansion of F is used, expressed around $\mathbf{c}_0$, the vector of the mean values of all the uncertainties:

$$F(\mathbf{c}) \approx F(\mathbf{c}_0) + \nabla F(\mathbf{c}_0)^\top (\mathbf{c} - \mathbf{c}_0) + \frac{1}{2} (\mathbf{c} - \mathbf{c}_0)^\top \nabla^2 F(\mathbf{c}_0) (\mathbf{c} - \mathbf{c}_0)$$

Higher-order Taylor expansions can also be utilized, but the computational accuracy is already sufficiently adequate in this case.

B.2 Mean Value Computation

Substituting the Taylor expansion into the integral of Eq. B.2, this becomes:

$$
\begin{aligned}
\mu_F =& F(\mathbf{c}_0) \int_{c_1} p(c_1)\, dc_1 \cdots \int_{c_M} p(c_M) dc_M \\
&+ \sum_{i=1}^{M} \frac{\partial F}{\partial c_i}(\mathbf{c}_0) \int (c_i - c_{0,i})\, p(c_i)\, dc_i \\
&+ \frac{1}{2} \sum_{i=1}^{M} \sum_{j=1}^{M} \frac{\partial^2 F}{\partial c_i \partial c_j}(\mathbf{c}_0) \int (c_i - c_{0,i})(c_j - c_{0,j})\, p(c_i) p(c_j)\, dc_i\, dc_j
\end{aligned}
\tag{B.5}
$$

Using the Eqs. B.4 and B.1, it is clear that terms like T of B.6 turn to zero:

$$
T = \int (c_i - c_{0,i})\, p(c_i) dc_i = \int c_i p(c_i) dc_i - c_{0,i} \int p(c_i) dc_i = c_{0,i} - c_{0,i} = 0 \tag{B.6}
$$

That leads Eq. B.5 to its final expression:

$$
\mu_F = F|_{\mathbf{c}_0} + \frac{1}{2} \sum_{i=1}^{M} \left.\frac{\partial^2 F}{\partial c_i^2}\right|_{\mathbf{c}_0} \sigma_i^2 \tag{B.7}
$$

B.3 Variance Computation

Similarly, the Taylor expansion is substituted into Eq. B.3, along with the computed expression of the mean value μ_F. The integral then becomes:

$$
\sigma_F^2 = \int \left(\nabla F(\mathbf{c}_0)^\top (\mathbf{c} - \mathbf{c}_0) + \frac{1}{2} (\mathbf{c} - \mathbf{c}_0)^\top \nabla^2 F(\mathbf{c}_0)(\mathbf{c} - \mathbf{c}_0) - \frac{1}{2} \sum_{i=1}^{M} \left.\frac{\partial^2 F}{\partial c_i^2}\right|_{\mathbf{c}_0} \sigma_i^2 \right)^2 p(\mathbf{c}) d\mathbf{c}
$$

Inside the brackets is the square of the sum of three terms, thus resulting in six terms, which are solved separately:

$$
\begin{aligned}
\sigma_F^2 = &\underbrace{\int \left[\sum_{i=1}^{M} \frac{dF}{dc_i}\left(c_i - c_{0,i}\right)\right]^2 p(\mathbf{c})\, d\mathbf{c}}_{\sigma_1} \\
&+ \underbrace{\int \left[\sum_{k=1}^{M} \frac{dF}{dc_k}\left(c_k - c_{0,k}\right)\right] \left[\sum_{i=1}^{M}\sum_{j=1}^{M} \frac{d^2F}{dc_i dc_j}\left(c_i - c_{0,i}\right)\left(c_j - c_{0,j}\right)\right] p(\mathbf{c})\, d\mathbf{c}}_{\sigma_2} \\
&+ \underbrace{\frac{1}{4}\int \left[\sum_{i=1}^{M}\sum_{j=1}^{M} \frac{d^2F}{dc_i dc_j}\left(c_i - c_{0,i}\right)\left(c_j - c_{0,j}\right)\right]^2 p(\mathbf{c})\, d\mathbf{c}}_{\sigma_3} \\
&- \underbrace{\int \left[\sum_{k=1}^{M} \frac{dF}{dc_k}\left(c_k - c_{0,k}\right)\right] \left[\sum_{i=1}^{M} \frac{d^2F}{dc_i^2}\sigma_i^2\right] p(\mathbf{c})\, d\mathbf{c}}_{\sigma_4} \\
&- \underbrace{\frac{1}{2}\int \left[\sum_{i=1}^{M}\sum_{j=1}^{M} \frac{d^2F}{dc_i dc_j}\left(c_i - c_{0,i}\right)\left(c_j - c_{0,j}\right)\right] \left[\sum_{k=1}^{M} \frac{d^2F}{dc_k^2}\sigma_k^2\right] p(\mathbf{c})\, d\mathbf{c}}_{\sigma_5} \\
&+ \underbrace{\frac{1}{4}\int \left[\sum_{i=1}^{M} \frac{d^2F}{dc_i^2}\sigma_i^2\right]^2 p(\mathbf{c})\, d\mathbf{c}}_{\sigma_6}
\end{aligned}
\tag{B.8}
$$

The first term becomes:

$$
\begin{aligned}
\sigma_1 &= \int \left[\sum_{i=1}^{M} \frac{dF}{dc_i}\left(c_i - c_{0,i}\right)\right] \left[\sum_{j=1}^{M} \frac{dF}{dc_j}\left(c_j - c_{0,j}\right)\right] p(\mathbf{c})\, d\mathbf{c} \\
&= \int \left[\left(\frac{dF}{dc_1}\right)^2 \left(c_1 - c_{0,1}\right)^2 + \left(\frac{dF}{dc_2}\right)^2 \left(c_2 - c_{0,2}\right)^2 + \cdots\right] p(\mathbf{c})\, d\mathbf{c} \\
&= \sum_{i=1}^{M} \left[\frac{dF}{dc_i}\right]^2 \sigma_i^2
\end{aligned}
\tag{B.9}
$$

after eliminating the null terms as Eq.B.6 dictates. The rest terms are solved similarly:

$$
\begin{aligned}
\sigma_2 &= \int \left[\sum_{k=1}^{M} \frac{dF}{dc_k} \left(c_k - c_{0,k} \right) \right] \left[\sum_{i=1}^{M} \sum_{j=1}^{M} \frac{d^2F}{dc_i dc_j} \left(c_i - c_{0,i} \right) \left(c_j - c_{0,j} \right) \right] p(\mathbf{c}) \, d\mathbf{c} \\
&= \int \Bigg\{ \Big[\frac{dF}{dc_1}(c_1 - c_{0,1}) + \frac{dF}{dc_2}(c_2 - c_{0,2}) + \cdots \Big] \\
&\qquad \times \Big[\frac{d^2F}{dc_1^2}(c_1 - c_{0,1})^2 + 2\frac{d^2F}{dc_1 dc_2}(c_1 - c_{0,1})(c_2 - c_{0,2}) + \cdots \Big] \Bigg\} p(\mathbf{c}) \, d\mathbf{c} \\
&= \sum_{i=1}^{M} \frac{dF}{dc_i} \frac{d^2F}{dc_i^2} \gamma_i
\end{aligned}
\tag{B.10}
$$

$$
\begin{aligned}
\sigma_3 &= \frac{1}{4} \int \left[\sum_{i=1}^{M} \sum_{j=1}^{M} \frac{d^2F}{dc_i dc_j} \left(c_i - c_{0,i} \right) \left(c_j - c_{0,j} \right) \right]^2 p(\mathbf{c}) \, d\mathbf{c} \\
&= \frac{1}{4} \int \Bigg\{ \Big[\frac{d^2F}{dc_1^2}(c_1 - c_{0,1})^2 + 2\frac{d^2F}{dc_1 dc_2}(c_1 - c_{0,1})(c_2 - c_{0,2}) + \cdots \Big] \\
&\qquad \times \Big[\frac{d^2F}{dc_1^2}(c_1 - c_{0,1})^2 + 2\frac{d^2F}{dc_1 dc_2}(c_1 - c_{0,1})(c_2 - c_{0,2}) + \cdots \Big] \Bigg\} p(\mathbf{c}) \, d\mathbf{c} \\
&= \frac{1}{4} \sum_{i=1}^{M} \left[\frac{d^2F}{dc_i^2} \right]^2 \sigma_i^4 + \frac{1}{2} \sum_{i=1}^{M} \sum_{\substack{j=1 \\ j \neq i}}^{M} \left[\frac{d^2F}{dc_i dc_j} \right]^2 \sigma_i^2 \sigma_j^2 \\
&\quad + \frac{1}{4} \sum_{i=1}^{M} \sum_{\substack{j=1 \\ j \neq i}}^{M} \left[\frac{d^2F}{dc_i^2} \right]^2 \sigma_i^2 \left[\frac{d^2F}{dc_j^2} \right]^2 \sigma_j^2
\end{aligned}
\tag{B.11}
$$

$$
\begin{aligned}
\sigma_4 &= -\int \left[\sum_{k=1}^{M} \frac{dF}{dc_k} \left(c_k - c_{0,k} \right) \right] \left[\sum_{i=1}^{M} \frac{d^2F}{dc_i^2} \sigma_i^2 \right] p(\mathbf{c}) \, d\mathbf{c} \\
&= -\sum_{i=1}^{M} \frac{d^2F}{dc_i^2} \sigma_i^2 \int \left[\sum_{k=1}^{M} \frac{dF}{dc_k} \left(c_k - c_{0,k} \right) \right] p(\mathbf{c}) \, d\mathbf{c} \\
&= 0
\end{aligned}
\tag{B.12}
$$

$$\begin{aligned}\sigma_5 &= -\frac{1}{2}\int\left[\sum_{i=1}^{M}\sum_{j=1}^{M}\frac{d^2F}{dc_idc_j}\left(c_i-c_{0,i}\right)\left(c_j-c_{0,j}\right)\right]\left[\sum_{k=1}^{M}\frac{d^2F}{dc_k^2}\sigma_k^2\right]p(\mathbf{c})\,d\mathbf{c}\\ &= -\frac{1}{2}\left[\sum_{k=1}^{M}\frac{d^2F}{dc_k^2}\sigma_k^2\right]\int\left[\sum_{i=1}^{M}\sum_{j=1}^{M}\frac{d^2F}{dc_idc_j}\left(c_i-c_{0,i}\right)\left(c_j-c_{0,j}\right)\right]p(\mathbf{c})\,d\mathbf{c}\\ &= -\frac{1}{2}\left[\sum_{k=1}^{M}\frac{d^2F}{dc_k^2}\sigma_k^2\right]\left[\sum_{k=1}^{M}\frac{d^2F}{dc_k^2}\sigma_k^2\right]\end{aligned}\tag{B.13}$$

$$\sigma_6 = \frac{1}{4}\int\left[\sum_{i=1}^{M}\frac{d^2F}{dc_i^2}\sigma_i^2\right]^2 p(\mathbf{c})\,d\mathbf{c} = \frac{1}{4}\left[\sum_{i=1}^{M}\frac{d^2F}{dc_i^2}\sigma_i^2\right]^2\tag{B.14}$$

Summing up the terms σ_5 and σ_6:

$$\begin{aligned}\sigma_{56} = \sigma_5+\sigma_6 &= -\frac{1}{4}\left[\sum_{i=1}^{M}\frac{d^2F}{dc_i^2}\sigma_i^2\right]\left[\sum_{i=1}^{M}\frac{d^2F}{dc_i^2}\sigma_i^2\right]\\ &= -\frac{1}{4}\sum_{i=1}^{M}\left[\frac{d^2F}{dc_i^2}\right]^2\sigma_i^4-\frac{1}{4}\sum_{i=1}^{M}\sum_{\substack{j=1\\ j\neq i}}^{M}\left[\frac{d^2F}{dc_i^2}\right]\sigma_i^2\left[\frac{d^2F}{dc_j^2}\right]\sigma_j^2\end{aligned}\tag{B.15}$$

Summing up all terms of Eqs. B.9 to B.14, the variance is derived:

$$\begin{aligned}\sigma_F^2 =& \sum_{i=1}^{M}\left[\frac{dF}{dc_i}\right]^2\sigma_i^2+\frac{1}{2}\sum_{i=1}^{M}\sum_{j=1}^{M}\left[\frac{d^2F}{dc_idc_j}\right]^2\sigma_i^2\sigma_j^2+\\ &\sum_{i=1}^{M}\frac{dF}{dc_i}\frac{d^2F}{dc_i^2}\gamma_i+\frac{1}{4}\sum_{i=1}^{M}\left[\frac{d^2F}{dc_i^2}\right]^2\left(k_i-3\sigma_i^4\right)\end{aligned}\tag{B.16}$$

Since each uncertain variable follows a normal distribution, as was established in the definition of the third and fourth statistical moments, Eq. B.16 becomes:

$$\sigma_F^2 = \sum_{i=1}^{M}\left[\frac{dF}{dc_i}\right]^2\sigma_i^2+\frac{1}{2}\sum_{i=1}^{M}\sum_{j=1}^{M}\left[\frac{d^2F}{dc_idc_j}\right]^2\sigma_i^2\sigma_j^2$$

In this thesis the standard deviation is used, i.e the square root of Eq. B.16:

$$\sigma_F = \sqrt{\sigma_F^2} = \sqrt{\sum_{i=1}^{M} \left[\frac{dF}{dc_i}\right]^2 \sigma_i^2 + \frac{1}{2} \sum_{i=1}^{M} \sum_{j=1}^{M} \left[\frac{d^2F}{dc_i dc_j}\right]^2 \sigma_i^2 \sigma_j^2}$$

Appendix C

Derivatives of the Fire Satellite System

This appendix presents methods for the computation of first- and second-order derivatives in the MD case of the FS. The focus at this stage is placed on the formulation and evaluation of the required sensitivity derivatives, independent of their subsequent use, be it UQ or MDO. The application of these specific derivative results within the UQ framework is addressed in Chapter 4. The desired system outputs of the QoIs are merged into a vector, denoted by $\vec{f}$:

$$\vec{f}^{\mathsf{T}} = \begin{bmatrix} \tau_{tot} & P_{tot} & A_{sa} \end{bmatrix} \tag{C.1}$$

$\vec{f}$ is then differentiated with respect to the variables of interest, which in this case constitute the uncertain input variable vector $\vec{c}$, of size $M = 9$:

$$\vec{c}^{\mathsf{T}} = \begin{bmatrix} H & C_d & L_a & \theta & L_{sp} & F_s & q & R_D & P_{other} \end{bmatrix} \tag{C.2}$$

C.1 First-Order Derivatives

Once the MDA system has converged according to the MDF approach, the resulting feasible state of the system is used to evaluate the derivative expressions presented in the following sections.

Finite Differences

The method of Finite Differences (FD) is applied as a reference to prove that the analytical methods presented next provide reliable results. In this case the forward differences will be applied, instead of central differences:

$$\left.\frac{df}{dc}\right|_{c_0} = \lim_{e \to 0} \frac{f(c_0 + e) - f(c_0)}{e} \tag{C.3}$$

The *Forward Differences* method, as stated in Eq. C.3 requires the computation of the QoI at the mean uncertain variable vector $\vec{c}_0$, which is comprised of the mean values of each uncertainty. Then, the QoI are evaluated M more times, each for a change in the value of a single variable, by a margin of e_i. The values of e_i must be really low, but not small enough for the derivative to lose computational accuracy. For the calculation of FD for every variable, different values apply for the e_i. This method's evaluation cost is high, as the complete MDA must be solved to convergence for each term of the FD.

Analytical Methods of Differentiation

To avoid the high cost of the FD, the system is differentiated analytically, with two methods: the DD and the Adjoint Method (AM) of differentiation. The QoIs are functions both of the uncertainties $c_i, i = 1, \ldots, 9$ and of the coupled functions I_{max}, I_{min} and P_{ACS}, which will now be denoted as $Y_j, i = 1, \ldots, N_Y$:

$$\vec{f}(\vec{c}, \vec{Y}(\vec{c}))$$

That means the derivatives with respect to $\vec{c}$ will be:

$$\frac{d\vec{f}}{d\vec{c}} = \frac{\partial \vec{f}}{\partial \vec{c}} + \frac{\partial \vec{f}}{\partial \vec{Y}} \frac{d\vec{Y}}{d\vec{c}} \tag{C.4}$$

Every partial derivative presented in this chapter can be directly extracted from the MDA system state primal equations, while the total derivatives-denoted by the symbol d of differentiation-must be computed.

Having expressed the derivatives of the objective functions, it is necessary to introduce a second set of functions needed for derivative evaluation: the Residual functions measure the deviation from exact satisfaction of the governing equations and must be null at convergence:

$$\vec{R}(\vec{c}, \vec{Y}) = 0$$

The residuals of the FS case are defined by the MD system and are presented in the following. Feasibility requires that the residuals be zero, together with all their higher-order derivatives:

$$\frac{d\vec{R}}{d\vec{c}} = \frac{\partial \vec{R}}{\partial \vec{c}} + \frac{\partial \vec{R}}{\partial \vec{Y}} \frac{d\vec{Y}}{d\vec{c}} = 0 \tag{C.5}$$

The coupled functions' derivatives are then expressed as:

$$\frac{d\vec{Y}}{d\vec{c}} = -\left(\frac{\partial \vec{R}}{\partial \vec{Y}}\right)^{-1} \frac{\partial \vec{R}}{\partial \vec{c}} \tag{C.6}$$

Substituting to Eq. C.4, the entire system of operations is acquired:

$$\frac{d\vec{f}}{d\vec{c}} = \frac{\partial \vec{f}}{\partial \vec{c}} - \frac{\partial \vec{f}}{\partial \vec{Y}} \left(\frac{\partial \vec{R}}{\partial \vec{Y}}\right)^{-1} \frac{\partial \vec{R}}{\partial \vec{c}} \tag{C.7}$$

C.1.1 Residuals of the FS System

The residual functions are reformulated expressions of the MD state primal equations. For each coupled function Y_i, a residual R_i is extracted from the primal system. To provide an example, in the scenario where $I_x = I_{max}$, the first residual function is obtained from the equation which defines the moment of inertia I_x, found in Eqs. A.30 :

$$R_1 = I_{sa,X} - m_{sa}\left(\frac{1}{12}\left(L^2 + t^2\right) + \left(D + \frac{L}{2}\right)^2\right) = 0 \tag{C.8}$$

Similarly, using Eq. A.20 the second residual is then:

$$R_2 = P_{ACS} - \tau_{tot}\omega_{max} - 3P_{hold} = 0 \tag{C.9}$$

The expression A.19 for τ_{tot} gives rise to two primary scenarios. Looking at Eqs. A.12 and A.13, it becomes clear that these scenarios subdivide into nine possible cases describing the system, depending on the relative magnitudes of the torques τ_{slew} or τ_{dist}, as well as the moments of inertia.

- **If** $\tau_{tot} = \tau_{slew}$, Eq. A.12 shows that there are three possibilities, as to which moment of inertia is the largest.
- **If** $\tau_{tot} = \tau_{dist}$, the role the moments of inertia play is in the gravitational torque τ_g of Eq. A.13. In this case six possibilities arise, in the combinations of the term $(I_{max} - I_{min})$.

The nine possible routes for the computation of the derivatives are then:

$$\tau_{tot} = \begin{cases} \tau_{slew}, \begin{cases} I_{max} = I_x \\ I_{max} = I_y \\ I_{max} = I_z \end{cases} \\ \tau_{dist}, \begin{cases} I_{max} = I_x \begin{cases} I_{min} = I_y \\ I_{min} = I_z \end{cases} \\ I_{max} = I_y \begin{cases} I_{min} = I_x \\ I_{min} = I_z \end{cases} \\ I_{max} = I_z \begin{cases} I_{min} = I_x \\ I_{min} = I_y \end{cases} \end{cases} \end{cases} \tag{C.10}$$

In the first branch of C.10 only one moment of inertia factors in the system, and in the second branch, a pair is used instead. Therefore, the vector $\vec{Y}$ has the following possible forms:

$$\vec{Y} = \begin{bmatrix} I_{\max} \\ P_{ACS} \end{bmatrix} \quad \text{or} \quad \vec{Y} = \begin{bmatrix} I_{\max} \\ I_{\min} \\ P_{ACS} \end{bmatrix} \tag{C.11}$$

When $\tau_{tot} = \tau_{dist}$, an additional residual function is inserted. For the case of $I_{min} = I_z$, the three residuals are:

$$\begin{aligned} R_1 =& I_{sa,X} - m_{sa}\left(\frac{1}{12}\left(L^2 + t^2\right) + \left(D + \frac{L}{2}\right)^2\right) = 0 \\ R_2 =& I_{sa,Z} - m_{sa}\left(\frac{1}{12}\left(L^2 + W^2\right) + \left(D + \frac{L}{2}\right)^2\right) = 0 \\ R_3 =& P_{ACS} - \tau_{tot}\omega_{max} - 3P_{hold} = 0 \end{aligned} \tag{C.12}$$

C.1.2 Constructing the Partial Derivatives

This section presents the way in which all the elements of the aforementioned matrices', namely the partial derivatives, are extracted from the primal system of the FS. Without loss of generality, every function is assumed to depend on all nine uncertain variables, plus the coupled functions, as the terms $\frac{\partial f}{\partial Y}, \frac{\partial R}{\partial Y}$ dictate. That leads, for every function, to a gradient of size $M+1$, providing 10 partial derivatives.

Firstly, the objective function $f_2 = P_{tot}$ is considered. Equation A.21 shows that P_{tot} is dependent on the coupled function P_{ACS}, and the uncertain variable P_{other}.

The differential of P_{tot} is then:

$$dP_{tot} = \frac{\partial P_{tot}}{\partial P_{ACS}} dP_{ACS} + \frac{\partial P_{tot}}{\partial P_{other}} dP_{other} = dP_{ACS} + dP_{other} \tag{C.13}$$

In order to proceed with the calculations, the computation of the derivative of the coupled function $Y = P_{ACS}$ is needed. The differential deconstruction of the coupled functions is a necessary step no matter the method of gradient analysis.

Differentials of Coupled Functions

The function of P_{ACS} is expanded through the third residual of equation C.12, which is also the equation A.20 from the primal presentation. It is clear that P_{ACS} is a function of τ_{tot}. How the expansion proceeds depends on which is larger, the τ_{slew} or τ_{dist}. It has been explained that from this point the analysis follows one of nine possible cases. To provide an example, the scenario of $\tau_{tot} = \tau_{slew}$, and $I_{max} = I_x$ is considered. The derivative of P_{ACS} is then:

$$dP_{ACS} = \frac{\partial P_{ACS}}{\partial \tau_{slew}} d\tau_{slew}$$

and by expanding the differential of τ_{slew}, the total differential of P_{ACS} is presented:

$$dP_{\mathrm{ACS}} = \frac{\partial P_{\mathrm{ACS}}}{\partial \tau_{\mathrm{slew}}} \left(\frac{\partial \tau_{\mathrm{slew}}}{\partial I_{max}} dI_{max} + \frac{\partial \tau_{\mathrm{slew}}}{\partial \theta_{\mathrm{slew}}} \left(\frac{\partial \theta_{\mathrm{slew}}}{\partial H} dH \right)_{d\theta_{slew}} \right)_{d\tau_{slew}} \tag{C.14}$$

The notation of each bracket denotes the differential it encloses. The differentiation with respect to every variable c_i is straightforward. The derivative is then,

$$\frac{dP_{ACS}}{dc_i} = \frac{\partial P_{ACS}}{\partial \tau_{slew}} \left(\frac{\partial \tau_{slew}}{\partial I_{max}} \frac{dI_{max}}{dc_i} + \frac{\partial \tau_{slew}}{\partial \theta_{slew}} \left(\frac{\partial \theta_{slew}}{\partial H} \frac{dH}{dc_i} \right)_{d\theta_{slew}} \right)_{d\tau_{slew}}$$

Since the uncertainties are independent variables, every term of $\frac{dc_i}{dc_j}$ acts as the Kronecker delta δ_{ij}, i.e:

$$\frac{dc_i}{dc_j} = \delta_{ij} = \begin{cases} 1, & \text{if } i = j \\ 0, & \text{if } i \neq j \end{cases}$$

That means that for the derivative with respect to H the expression becomes

$$\frac{dP_{ACS}}{dH} = \frac{\partial P_{ACS}}{\partial \tau_{slew}} \left(\frac{\partial \tau_{slew}}{\partial I_x} \frac{dI_x}{dH} + \frac{\partial \tau_{slew}}{\partial \theta_{slew}} \left(\frac{\partial \theta_{slew}}{\partial H} \right)_{d\theta_{slew}} \right)_{d\tau_{slew}}$$

while, for every other uncertain variable c_j, the derivative is simply

$$\frac{dP_{ACS}}{dc_j} = \frac{\partial P_{ACS}}{\partial \tau_{slew}} \left(\frac{\partial \tau_{slew}}{\partial I_{max}} \frac{dI_{max}}{dc_j} \right)_{d\tau_{slew}}$$

The only derivatives that can not be expanded any further are the coupled functions', as is shown with dI_{max} above. It is clear that all the derivatives of P_{ACS} are also dependent on the derivatives of the I_{max}, which in this example is the I_x. The differential of I_x is acquired the same way, starting from the respective residual, which in this case is also the primal state Eq. A.30. The total differential is derived as:

$$\begin{aligned} dI_x = \frac{\partial I_x}{\partial A_{sa}} \Bigg(\frac{\partial A_{sa}}{\partial P_{sa}} \Bigg(\frac{\partial P_{sa}}{\partial P_{tot}} \Big(\frac{\partial P_{tot}}{\partial P_{ACS}} dP_{ACS} + \frac{\partial P_{tot}}{\partial P_{other}} dP_{other} \Big)_{dP_{tot}} \\ + \frac{\partial P_{sa}}{\partial T_d} \Big(\frac{\partial T_d}{\partial \Delta T_{orbit}} \frac{\partial \Delta T_{orbit}}{\partial H} dH + \frac{\partial T_d}{\partial \Delta T_{eclipse}} \frac{\partial \Delta T_{eclipse}}{\partial H} dH \Big)_{dT_d} \\ + \frac{\partial P_{sa}}{\partial T_e} \Big(\frac{\partial T_e}{\partial \Delta T_{eclipse}} \frac{\partial \Delta T_{eclipse}}{\partial H} dH \Big)_{dT_e} \Bigg)_{dP_{sa}} \\ + \frac{\partial A_{sa}}{\partial P_{eol}} \Bigg(\frac{\partial P_{eol}}{\partial P_{bol}} \Big(\frac{\partial P_{bol}}{\partial F_s} dF_s \Big)_{dP_{bol}} \Bigg)_{dP_{eol}} \Bigg)_{dA_{sa}} \end{aligned} \tag{C.15}$$

The final outcome is that for every derivative computation, a system of 2×2 must be solved, for the values of the derivatives of the coupled functions to be acquired:

$$\begin{aligned} \frac{dI_x}{dc_i} &= prt1 \frac{dP_{ACS}}{dc_i} + prt2 \\ \frac{dP_{ACS}}{dx_i} &= prt3 \frac{dI_x}{dc_i} + prt4 \end{aligned}$$

The *prt_i* terms are the partial derivatives explained above, written symbolically since their values have been presented at this point. The terms $prt1, prt3$ are the partial derivatives of one coupled function with respect to the other, and $prt2, prt4$ are the partial derivatives of each coupled function with respect to the uncertainty c_i- which are null for the c_i the function is not dependent on. The system is expressed in matrix form, to show that it is identical to the one given by eq. C.6:

$$\begin{bmatrix} 1 & -prt1 \\ -prt3 & 1 \end{bmatrix} \begin{bmatrix} \frac{dI_x}{dc_i} \\ \frac{dP_{ACS}}{dc_i} \end{bmatrix} = \begin{bmatrix} prt2 \\ prt4 \end{bmatrix} \tag{C.16}$$

The matrix on the left remains the same no matter the uncertainty the system is solved for. The column vector on the right side is dependent on the uncertainties, and when it is null, the coupled functions' derivatives are zero for that uncertainty. For a system of this size, the solution can be obtained analytically by inverting the matrix on the left-hand side:

$$\begin{bmatrix} \frac{dI_x}{dc_i} \\ \frac{dP_{ACS}}{dc_i} \end{bmatrix} = \begin{bmatrix} 1 & -prt1 \\ -prt3 & 1 \end{bmatrix}^{-1} \begin{bmatrix} prt2 \\ prt4 \end{bmatrix}$$

The system above is formed in the same way for the other possible routes $I_{max} = I_y$ or I_z. A much more complex system is formed when $\tau_{tot} = \tau_{dist}$. In that case, the four disturbing torques are examined as stated in the equations A.15 to A.17. The total differential of P_{ACS} in this case is:

$$\begin{aligned} dP_{ACS} =& \frac{\partial P_{ACS}}{\partial \tau_{dist}} \left(\frac{\partial \tau_{dist}}{\partial \tau_g} \left(\frac{\partial \tau_g}{\partial I_{max}} dI_{max} + \frac{\partial \tau_g}{\partial I_{min}} dI_{min} + \frac{\partial \tau_g}{\partial \theta} d\theta + \frac{\partial \tau_g}{\partial H} dH \right)_{d\tau_g} \right. \\ & + \frac{\partial \tau_{dist}}{\partial \tau_{sp}} \left(\frac{\partial \tau_{sp}}{\partial F_s} dF_s + \frac{\partial \tau_g}{\partial L_{sp}} dL_{sp} + \frac{\partial \tau_{sp}}{\partial q} dq \right)_{d\tau_{sp}} \\ & + \frac{\partial \tau_{dist}}{\partial \tau_m} \left(\frac{\partial \tau_m}{\partial R_D} dR_D + \frac{\partial \tau_m}{\partial H} dH \right)_{d\tau_m} \\ & \left. + \frac{\partial \tau_{dist}}{\partial \tau_a} \left(\frac{\partial \tau_a}{\partial L_a} dL_a + \frac{\partial \tau_a}{\partial C_d} dC_d + \frac{\partial \tau_a}{\partial H} dH \right)_{d\tau_a} \right)_{d\tau_{dist}} \end{aligned} \tag{C.17}$$

The coupled functions of moments of inertia appear in the gravity gradient torque, eq. A.13, in the term $(I_{max} - I_{min})$. That means that now the coupled variables are the power P_{ACS}, and two moments of inertia I_{min} and I_{max}. The three equations needed are, then,

$$\begin{aligned} \frac{dI_{max}}{dc_i} &= prt1 \frac{dP_{ACS}}{dc_i} + prt2 \\ \frac{dI_{min}}{dc_i} &= prt3 \frac{dP_{ACS}}{dc_i} + prt4 \\ \frac{dP_{ACS}}{dc_i} &= prt5 \frac{dI_{max}}{dc_i} + prt6 \frac{dI_{min}}{dc_i} + prt7 \end{aligned} \tag{C.18}$$

and the coupled system becomes:

$$\begin{bmatrix} 1 & 0 & -prt1 \\ 0 & 1 & -prt3 \\ -prt5 & -prt6 & 1 \end{bmatrix} \begin{bmatrix} \frac{dI_{max}}{dc_i} \\ \frac{dI_{min}}{dc_i} \\ \frac{dP_{ACS}}{dc_i} \end{bmatrix} = \begin{bmatrix} prt2 \\ prt4 \\ prt7 \end{bmatrix}$$

As has already been stated the 2×2 or the 3×3 matrix remains the same for every uncertain variable derivative. What changes per variable is the column vector on the right hand side, so in total, the inverse of the matrix is multiplied to nine column vectors per optimization iteration.

C.1.3 The derivatives of the QoIs

Using the computed derivatives of the coupled functions, the derivatives of the QoI are calculated. The derivative of $f_2 = P_{tot}$ has been expressed in eq. C.13. The derivative of $f_1 = \tau_{tot}$ is the most complex one, as its general expression depends on the scenario of the case. There are nine possibilities, subdivided from two overarching branches.

$$d\tau_{tot} = \begin{cases} d\tau_{slew} = \dfrac{\partial \tau_{slew}}{\partial I_{max}} dI_{max} + \dfrac{\partial \tau_{slew}}{\partial H} dH \\ d\tau_{dist} = \dfrac{\partial \tau_{dist}}{\partial I_{max}} dI_{max} + \dfrac{\partial \tau_{dist}}{\partial I_{min}} dI_{min} \\ \qquad + \dfrac{\partial \tau_{dist}}{\partial H} dH + \dfrac{\partial \tau_{dist}}{\partial F_s} dF_s \\ \qquad + \dfrac{\partial \tau_{dist}}{\partial \theta} d\theta + \dfrac{\partial \tau_{dist}}{\partial L_{sp}} dL_{sp} \\ \qquad + \dfrac{\partial \tau_{dist}}{\partial q} dq + \dfrac{\partial \tau_{dist}}{\partial R_D} dR_D \\ \qquad + \dfrac{\partial \tau_{dist}}{\partial L_a} dL_a + \dfrac{\partial \tau_{dist}}{\partial C_d} dC_d \end{cases} \tag{C.19}$$

Going through almost the entire power analysis, starting from the equation A.27, the derivative of $f_3 = A_{sa}$ is obtained:

$$
\begin{aligned}
dA_{sa} = & \frac{\partial A_{sa}}{\partial P_{sa}} \left(\frac{\partial P_{sa}}{\partial P_{tot}} \left(\frac{\partial P_{tot}}{\partial P_{ACS}} dP_{ACS} + \frac{\partial P_{tot}}{\partial P_{other}} dP_{other} \right)_{dP_{tot}} \right. \\
& + \frac{\partial P_{sa}}{\partial T_d} \left(\frac{\partial T_d}{\partial \Delta T_{orbit}} \frac{\partial \Delta T_{orbit}}{\partial H} dH + \frac{\partial T_d}{\partial \Delta T_{eclipse}} \frac{\partial \Delta T_{ecclipse}}{\partial H} dH \right)_{dT_d} \\
& \left. + \frac{\partial P_{sa}}{\partial T_e} \left(\frac{\partial T_e}{\partial \Delta T_{eclipse}} \frac{\partial \Delta T_{ecclipse}}{\partial H} dH \right)_{dT_e} \right)_{dP_{sa}} \\
& + \frac{\partial A_{sa}}{\partial P_{eol}} \left(\frac{\partial P_{eol}}{\partial P_{bol}} \left(\frac{\partial P_{bol}}{\partial F_s} dF_s \right)_{dP_{bol}} \right)_{dP_{eol}}
\end{aligned}
\tag{C.20}
$$

Factoring out the terms to form sums of each derivative

$$
\begin{aligned}
dA_{sa} = & \frac{\partial A_{sa}}{\partial P_{sa}} \frac{\partial P_{sa}}{\partial P_{tot}} \frac{\partial P_{tot}}{\partial P_{ACS}} dP_{ACS} \\
& + \frac{\partial A_{sa}}{\partial P_{sa}} \frac{\partial P_{sa}}{\partial P_{tot}} \frac{\partial P_{tot}}{\partial P_{other}} dP_{other} \\
& + \frac{\partial A_{sa}}{\partial P_{sa}} \left(\frac{\partial P_{sa}}{\partial T_d} \frac{\partial T_d}{\partial H} + \frac{\partial P_{sa}}{\partial T_e} \frac{\partial T_e}{\partial H} \right) dH \\
& + \frac{\partial A_{sa}}{\partial P_{eol}} \frac{\partial P_{eol}}{\partial P_{bol}} \frac{\partial P_{bol}}{\partial F_s} dF_s
\end{aligned}
\tag{C.21}
$$

At this point the partial derivatives can be placed in the systems needed for either the DD or the AM.

C.1.4 Direct Differentiation

The DD approach handles the derivatives of the coupled functions Y_i first, by solving Eq. C.6 and then substituting the derivatives in Eq. C.4. Tables C.1 to C.3 compare the results of this analysis for the three QoIs to those of the FD method. It is clear the results are practically identical, hence the method followed is reliable.

Size of Operations

Using the FD method, the MD primal system has to be solved $M + 1$ times. Applying DD for the coupled derivatives instead, the primal is solved once, but M systems of size $N_Y \times N_Y$ must be solved. A better approach is required, provided in the following method.

	$dP_{tot,FD}$	$dP_{tot,DD}$	$divergence(\%)$
H	-3.57e-07	-3.57e-07	2.69e-04
P_{other}	1	1	-3.32e-09
F_s	1.33e-06	1.33e-06	-1.03e-02
θ	4.79e-06	4.79e-06	-2.20e-02
L_{sp}	9.31e-04	9.31e-04	-1.40e-03
q	1.24e-03	1.24e-03	-3.81e-04
R_D	5.00e-07	4.99e-07	-2.13e-01
L_a	3.99	3.99e	-1.06e-07
C_d	7.98	7.98e	-3.44e-07

Table C.1: P_{tot} derivative comparison, FD vs. DD

	$d\tau_{tot,FD}$	$d\tau_{tot,DD}$	$divergence(\%)$
H	-5.67e-10	-5.67e-10	2.68e-04
P_{other}	-9.02e-14	-9.05e-14	2.83e-01
F_s	2.12e-09	2.12e-09	-1.52e-05
θ	7.62e-09	7.62e-09	-2.79e-04
L_{sp}	1.48e-06	1.48e-06	-6.02e-04
q	1.98e-06	1.98e-06	-2.07e-04
R_D	7.94e-10	7.94e-10	-1.59e-03
L_a	6.35e-03	6.35e-03	-1.46e-07
C_d	1.27e-02	1.27e-02	-2.20e-07

Table C.2: τ_{tot} derivative comparison, FD vs. DD

C.1.5 Adjoint Method of Differentiation

A focus must be placed on the matrices' multiplication that arise in the second term (T_2) of Eq.C.7:

$$T_2 = \frac{\partial \vec{f}}{\partial \vec{Y}} \left(\frac{\partial \vec{R}}{\partial \vec{Y}} \right)^{-1} \frac{\partial \vec{R}}{\partial \vec{c}} \tag{C.22}$$

Different results come from the order of operations as is presented below:

	$dA_{sa,FD}$	$dA_{sa,DD}$	$divergence(\%)$
H	-8.14e-08	-8.14e-08	3.16e-04
P_{other}	4.83e-03	4.83e-03	-6.33e-09
F_s	-3.68e-03	-3.68e-03	8.58e-05
θ	2.31e-08	2.31e-08	-9.49e-02
L_{sp}	4.50e-06	4.50e-06	-1.72e-03
q	6.00e-06	6.00e-06	-2.54e-03
R_D	2.43e-09	2.41e-09	-6.78e-01
L_a	1.93e-02	1.93e-02	-1.88e-07
C_d	3.85e-02	3.85e-02	-3.16e-07

Table C.3: A_{sa} derivative comparison, FD vs. DD

$$\underbrace{\frac{\partial \vec{f}}{\partial \vec{Y}} \mathrlap{\overbrace{\phantom{\left(\frac{\partial \vec{R}}{\partial \vec{Y}}\right)^{-1} \frac{\partial \vec{R}}{\partial \vec{c}}}}^{-\frac{d\vec{Y}}{d\vec{c}}}} \left(\frac{\partial \vec{R}}{\partial \vec{Y}}\right)^{-1}}_{\vec{\Psi}^T} \frac{\partial \vec{R}}{\partial \vec{c}}$$

Figure C.1: Difference between DD and AM.

The straight-forward way of DD first dictates the calculation of the product:

$$\left(\frac{\partial \vec{R}}{\partial \vec{Y}}\right)^{-1} \frac{\partial \vec{R}}{\partial \vec{c}} = -\frac{d\vec{Y}}{d\vec{c}}$$

which is then multiplied to the matrix $\frac{\partial \vec{f}}{\partial \vec{Y}}$. On the other side, the dot product of the first two matrices of T_2 is named the adjoint matrix (the transpose of the adjoint for that matter).

$$\frac{\partial \vec{f}}{\partial \vec{Y}} \left(\frac{\partial \vec{R}}{\partial \vec{Y}}\right)^{-1} = \Psi^T \tag{C.23}$$

Examining Eq.C.23, it is clear that the Adjoint Matrix is of size $N_Y \times N_f$. Expressing the matrix operations differently, the equation becomes:

$$\begin{aligned} \Psi^T &= \frac{\partial \vec{f}}{\partial \vec{Y}} \left(\frac{\partial \vec{R}}{\partial \vec{Y}} \right)^{-1} \\ \Leftrightarrow \left(\Psi^T \frac{\partial \vec{R}}{\partial \vec{Y}} \right)^T &= \left(\frac{\partial \vec{f}}{\partial \vec{Y}} \right)^T \\ \Leftrightarrow \left(\frac{\partial \vec{R}}{\partial \vec{Y}} \right)^T \Psi &= \left(\frac{\partial \vec{f}}{\partial \vec{Y}} \right)^T \end{aligned} \tag{C.24}$$

At the final expression of Eq. C.24, Ψ can be computed by solving the system iteratively, using methods like the *Gauss Seidel*. If the inverse of $\frac{\partial \vec{R}}{\partial \vec{Y}}$ is easily computed, which is true in this case, the first equation can be applied instead. The derivative of the objective function is then:

$$\frac{d\vec{f}}{d\vec{c}} = \frac{\partial \vec{f}}{\partial \vec{c}} - \Psi^T \frac{\partial \vec{R}}{\partial \vec{c}}$$

Again, the accuracy of the method is tested below, for the same 3 objective functions.

	$dP_{tot,FD}$	$dP_{tot,Adjoint}$	$divergence(\%)$
H	-3.57e-07	-3.57e-07	2.69e-04
P_{other}	1	1	-3.32e-09
F_s	1.33e-06	1.33e-06	-1.03e-02
θ	4.79e-06	4.79e-06	-2.20e-02
L_{sp}	9.31e-04	9.31e-04	-1.40e-03
q	1.24e-03	1.24e-03	-3.81e-04
R_D	5.00e-07	4.99e-07	-2.13e-01
L_a	3.99e+00	3.99e+00	-1.06e-07
C_d	7.98e+00	7.98e+00	-3.44e-07

Table C.4: P_{tot} derivative comparison, FD vs Adjoint Method

The results are the same as the ones provided by *DD*.

Benefit of the Adjoint Method

The order of operations applied for *DD* and *AM* presented in the term T_2 of C.22 is analyzed in Figs. C.2 and C.3 respectively.

The elements used are the same in each case, but when it comes to matrices multiplication, order matters. It is clear that after the first multiplication, the matrices are of same sizes for both cases. The difference between the *DD* and *AM*, and in the system's very cost is determined from which product is calculated first.

	$d\tau_{tot,FD}$	$d\tau_{tot,Adjoint}$	$divergence(\%)$
H	-5.67e-10	-5.67e-10	2.68e-04
P_{other}	-9.02e-14	-9.05e-14	2.83e-01
F_s	2.12e-09	2.12e-09	-1.52e-05
θ	7.62e-09	7.62e-09	-2.79e-04
L_{sp}	1.48e-06	1.48e-06	-6.02e-04
q	1.98e-06	1.98e-06	-2.07e-04
R_D	7.94e-10	7.94e-10	-1.59e-03
L_a	6.35e-03	6.35e-03	-1.46e-07
C_d	1.27e-02	1.27e-02	-2.20e-07

Table C.5: τ_{tot} derivative comparison, FD vs Adjoint Method

	$dA_{sa,FD}$	$dA_{sa,Adjoint}$	$divergence(\%)$
H	-8.14e-08	-8.14e-08	3.16e-04
P_{other}	4.83e-03	4.83e-03	-6.33e-09
F_s	-3.68e-03	-3.68e-03	8.58e-05
θ	2.31e-08	2.31e-08	-9.49e-02
L_{sp}	4.50e-06	4.50e-06	-1.72e-03
q	6.00e-06	6.00e-06	-2.54e-03
R_D	2.43e-09	2.41e-09	-6.78e-01
L_a	1.93e-02	1.93e-02	-1.88e-07
C_d	3.85e-02	3.85e-02	-3.16e-07

Table C.6: A_{sa} derivative comparison, FD vs Adjoint Method

$$(N_f \times N_Y) \cdot \underbrace{\Big((N_Y \times N_Y) \cdot (N_Y \times M)\Big)}_{\text{operations scale with } M} \Rightarrow (N_f \times N_Y) \cdot (N_Y \times M) \Rightarrow (N_f \times M)$$

Figure C.2: Direct Method Order of Operations

DD:
The dot product in brackets of Fig. C.2 computes N_Y element-products for each new element of the $(N_Y \times M)$ matrix, costing the solver a total of MN_Y^2 terms.

AM:
The brackets in Fig. C.3 also express N_Y element-products per element, but this time to construct a matrix of size $(N_f \times N_Y)$, costing a total of $N_f N_Y^2$ terms.

Both methods then are followed by a multiplication of scale $(N_f \times N_Y) \cdot (N_Y \times M)$. That multiplication demands N_Y element-products for each element of the final

$$\underbrace{\Big((N_f \times N_Y)\cdot(N_Y \times N_Y)\Big)}_{\text{operations scale with } N_f} \cdot (N_Y \times M) \Rightarrow (N_f \times N_Y)\cdot(N_Y \times M) \Rightarrow (N_f \times M)$$

Figure C.3: Adjoint Method Order of Operations

$(N_f \times M)$ matrix, so in total $N_Y M N_f$ terms.

The cost sum of the two steps is presented in Table C.8 for the two methods:

Size of Operations	
Direct	$MN_Y(N_Y + N_f)$
Adjoint	$N_f N_Y(N_Y + M)$

Table C.7: DD vs AM Costs.

The cost of the direct method scales with M, the size of the uncertain variables, while the adjoint method scales with N_f, the size of the QoI. The cost ratio of the direct method to that of the adjoint is:

$$\frac{DD_{cost}}{AM_{cost}} = \frac{MN_Y(N_Y + N_f)}{N_f N_Y(N_Y + M)} = \frac{M}{N_f}\frac{N_Y + N_f}{N_Y + M} = \frac{M}{N_f}\frac{1 + \frac{N_f}{N_Y}}{1 + \frac{M}{N_Y}}$$

That means that for very large scale systems, where $N_Y \to \infty$, the DD-to-AM cost ratio is $\frac{DD_{cost}}{AM_{cost}} \to \frac{M}{N_f}$. That is, as long as $M > N_f$, the adjoint method is the preferable choice. In the fire satellite case, $M = 9$ and $N_f = 3$ so the advantage of the adjoint method is considerate.

Derivatives Computation Cost Relative to the Primal System

The comparison of these methods' costs can be expressed with respect to the cost of the primal system's convergence: The DD method solves $M = 9$ systems of size $N_Y \times N_Y$. Each system has about the size of one primal convergence iteration. Therefore, as an informed reference, it can be said that:

$$\boxed{DDcost \approx 9\ primal_{cost}}$$

Consequently, the AM cost for this case specifically is:

$$\boxed{AM_{cost} \approx 9 \times \frac{AM_{cost}}{DD_{cost}} \times primal_{cost} \approx 6 \times primal_{cost}}$$

C.2 Second-Order Derivatives

The second-order derivatives are obtained by differentiating the Eqs. C.4 and C.5. Once more, every function- in this case, the partial derivative terms used in the first-order derivative computation- is regarded as a function of the coupled functions and the uncertainties. For the residual function, this gives:

$$\frac{d^2\vec{R}}{d\vec{c}^2} = \frac{d}{d\vec{c}}\left(\frac{\partial\vec{R}}{\partial\vec{c}}\right) + \frac{d}{d\vec{c}}\left(\frac{\partial\vec{R}}{\partial\vec{Y}}\right)\frac{d\vec{Y}}{d\vec{c}} + \frac{\partial\vec{R}}{\partial\vec{Y}}\frac{d}{d\vec{c}}\left(\frac{d\vec{Y}}{d\vec{c}}\right)$$

which, when expanding the terms become:

$$\begin{aligned}\frac{d^2\vec{R}}{d\vec{c}^2} &= \left(\frac{\partial^2\vec{R}}{\partial^2\vec{c}} + \frac{\partial^2\vec{R}}{\partial\vec{c}\partial\vec{Y}}\frac{d\vec{Y}}{d\vec{c}}\right) + \left(\frac{\partial^2\vec{R}}{\partial\vec{Y}\partial\vec{c}} + \frac{\partial^2\vec{R}}{\partial^2\vec{Y}}\frac{d\vec{Y}}{d\vec{c}}\right)\frac{d\vec{Y}}{d\vec{c}} + \frac{\partial\vec{R}}{\partial\vec{Y}}\left(\frac{d^2\vec{Y}}{d\vec{c}^2}\right) \\ &= \frac{d^2\vec{R}}{d\vec{c}^2} = \frac{\partial^2\vec{R}}{\partial^2\vec{c}} + 2\frac{\partial^2\vec{R}}{\partial\vec{c}\partial\vec{Y}}\frac{d\vec{Y}}{d\vec{c}} + \frac{\partial^2\vec{R}}{\partial^2\vec{Y}}\frac{d\vec{Y}}{d\vec{c}}\frac{d\vec{Y}}{d\vec{c}} + \frac{\partial\vec{R}}{\partial\vec{Y}}\frac{d^2\vec{Y}}{d\vec{c}^2}\end{aligned} \tag{C.25}$$

The procedure already becomes complex. The matrix $\frac{\partial\vec{R}}{\partial\vec{Y}}$ is now differentiated with respect to the coupled functions $\vec{Y}$ and becomes a tensor of three dimensions:

$$\frac{\partial^2\vec{R}}{\partial^2\vec{Y}} = \left\{\begin{bmatrix} 0 & 0 \\ \frac{\partial^2 R_2}{\partial Y_1^2} & 0 \end{bmatrix}, \quad \begin{bmatrix} 0 & \frac{\partial^2 R_1}{\partial Y_2^2} \\ 0 & 0 \end{bmatrix}\right\}$$

In order to avoid complexity, the operations will be expressed in element form as opposed to the full vector form. Thus, the second-order derivative with respect to the uncertainties c_i, c_j is:

$$\frac{d^2\vec{R}}{dc_i dc_j} = \frac{\partial^2\vec{R}}{\partial c_i\partial c_j} + \frac{\partial^2\vec{R}}{\partial c_i\partial\vec{Y}}\frac{d\vec{Y}}{dc_j} + \left(\frac{\partial^2\vec{R}}{\partial\vec{Y}\partial c_j} + \frac{\partial^2\vec{R}}{\partial^2\vec{Y}}\frac{d\vec{Y}}{dc_j}\right)\frac{d\vec{Y}}{dc_i} + \frac{\partial\vec{R}}{\partial\vec{Y}}\frac{d^2\vec{Y}}{dc_i dc_j} = 0 \tag{C.26}$$

The second-order total derivatives are then:

$$\frac{d^2\vec{Y}}{dc_i dc_j} = -\left(\frac{\partial\vec{R}}{\partial\vec{Y}}\right)^{-1}\left(\frac{\partial^2\vec{R}}{\partial c_i\partial c_j} + \frac{\partial^2\vec{R}}{\partial c_i\partial\vec{Y}}\frac{d\vec{Y}}{dc_j} + \left(\frac{\partial^2\vec{R}}{\partial\vec{Y}\partial c_j} + \frac{\partial^2\vec{R}}{\partial^2\vec{Y}}\frac{d\vec{Y}}{dc_j}\right)\frac{d\vec{Y}}{dc_i}\right) \tag{C.27}$$

The right-hand matrix is named $[B]$ for later reference.

$$\boldsymbol{B} = \left(\frac{\partial^2\vec{R}}{\partial c_i\partial c_j} + \frac{\partial^2\vec{R}}{\partial c_i\partial\vec{Y}}\frac{d\vec{Y}}{dc_j} + \left(\frac{\partial^2\vec{R}}{\partial\vec{Y}\partial c_j} + \frac{\partial^2\vec{R}}{\partial^2\vec{Y}}\frac{d\vec{Y}}{dc_j}\right)\frac{d\vec{Y}}{dc_i}\right)$$

For a fixed i, $[\mathbf{B}]$ is of size $N_Y \times M = N_Y \times 9$, where N_Y is the size of the coupled functions, 2 or 3 depending on the scenario. That is of course the same size as the second derivatives for each i element. The first term of $[B]$, for the fixed elements i, j is straightforward, a vector of size $N_Y \times 1$. The second term is, for $N_Y = 2$,

$$\frac{\partial^2\vec{R}}{\partial c_i\partial\vec{Y}}\frac{d\vec{Y}}{dc_j} = \begin{bmatrix} \frac{\partial R_1}{\partial c_i\partial Y_1} & \frac{\partial R_1}{\partial c_i\partial Y_2} \\ \frac{\partial R_2}{\partial c_i\partial Y_1} & \frac{\partial R_2}{\partial c_i\partial Y_2} \end{bmatrix} \begin{bmatrix} \frac{dY_1}{dc_j} \\ \frac{dY_2}{dc_j} \end{bmatrix} = \begin{bmatrix} \frac{\partial R_1}{\partial c_i\partial Y_1}\frac{dY_1}{dc_j} + \frac{\partial R_1}{\partial c_i\partial Y_2}\frac{dY_2}{dc_j} \\ \frac{\partial R_2}{\partial c_i\partial Y_1}\frac{dY_1}{dc_j} + \frac{\partial R_2}{\partial c_i\partial Y_2}\frac{dY_2}{dc_j} \end{bmatrix}$$

Next, the $\frac{\partial\vec{R}}{\partial\vec{Y}}$ matrix differentiated with respect to c_j multiplied with the derivatives of the coupled functions:

$$\frac{\partial^2\vec{R}}{\partial\vec{Y}\partial c_j}\frac{d\vec{Y}}{dc_i} = \begin{bmatrix} 0 & \frac{\partial R_1}{\partial Y_2\partial c_j} \\ \frac{\partial R_2}{\partial Y_1\partial c_j} & 0 \end{bmatrix} \begin{bmatrix} \frac{\partial Y_1}{\partial c_i} \\ \frac{\partial Y_2}{\partial c_i} \end{bmatrix} \rightarrow \begin{bmatrix} \frac{\partial R_1}{\partial Y_2\partial c_j}\frac{\partial Y_2}{\partial c_i} \\ \frac{\partial R_2}{\partial Y_1\partial c_j}\frac{\partial Y_1}{\partial c_i} \end{bmatrix}$$

The bothersome 3D tensor is multiplied with the derivative $\frac{d\vec{Y}}{d\vec{c_j}}$:

$$\frac{\partial^2\vec{R}}{\partial^2\vec{Y}} \cdot \frac{d\vec{Y}}{dc_j} = \left\{ \begin{bmatrix} 0 \\ \frac{\partial^2 R_2}{\partial Y_1\partial Y_1} \cdot \frac{dY_1}{dc_j} \end{bmatrix}, \quad \begin{bmatrix} \frac{\partial^2 R_1}{\partial Y_2\partial Y_2} \cdot \frac{dY_2}{dc_j} \\ 0 \end{bmatrix} \right\}$$

which is in fact a 2D matrix:

$$\frac{\partial^2\vec{R}}{\partial^2\vec{Y}} \cdot \frac{d\vec{Y}}{dc_j} = \begin{bmatrix} 0 & \frac{\partial R_1}{\partial Y_2\partial Y_2} \cdot \frac{dY_2}{dc_j} \\ \frac{\partial R_2}{\partial Y_1\partial Y_1} \cdot \frac{dY_1}{dc_j} & 0 \end{bmatrix}$$

Multiplying again, this time with $\frac{d\vec{Y}}{dc_i}$:

$$\frac{\partial^2 \vec{R}}{\partial^2 \vec{Y}} \cdot \frac{d\vec{Y}}{dc_j} \frac{d\vec{Y}}{dc_i} = \begin{bmatrix} \frac{\partial R_1}{\partial Y_2 \partial Y_2} \frac{dY_2}{dc_j} \frac{dY_2}{dc_i} \\ \frac{\partial R_2}{\partial Y_1 \partial Y_1} \frac{dY_1}{dc_j} \frac{dY_1}{dc_i} \end{bmatrix}$$

Similar operations take place when $N_Y = 3$, with the 3D matrix being:

$$\frac{\partial^2 \vec{R}}{\partial^2 \vec{Y}} = \left\{ \begin{bmatrix} 0 & 0 & 0 \\ 0 & 0 & 0 \\ \frac{\partial R_3}{\partial Y_1 \partial Y_1} & \frac{\partial R_3}{\partial Y_1 \partial Y_1} & 0 \end{bmatrix}, \begin{bmatrix} 0 & 0 & 0 \\ 0 & 0 & 0 \\ \frac{\partial R_3}{\partial Y_1 \partial Y_2} & \frac{\partial R_3}{\partial Y_1 \partial Y_2} & 0 \end{bmatrix}, \begin{bmatrix} 0 & 0 & \frac{\partial R_1}{\partial Y_3 \partial Y_3} \\ 0 & 0 & \frac{\partial R_2}{\partial Y_3 \partial Y_3} \\ 0 & 0 & 0 \end{bmatrix} \right\}$$

Finally, the $N_Y \times N_Y$ system needed to compute the i, j elements of the second-order derivatives of the coupled functions Y_1, Y_2, are presented below:

$$\begin{bmatrix} \frac{d^2 Y_1}{dc_i dc_j} \\ \frac{d^2 Y_2}{dc_i dc_j} \end{bmatrix} = - \begin{bmatrix} 1 & \frac{\partial R_1}{\partial Y_2} \\ \frac{\partial R_2}{\partial Y_1} & 1 \end{bmatrix}^{-1} \begin{bmatrix} \frac{\partial^2 R_1}{\partial c_i \partial Y_2} \frac{dY_2}{dc_j} + \frac{\partial^2 R_1}{\partial c_i \partial c_j} + \frac{\partial^2 R_1}{\partial Y_2 \partial c_j} \frac{dY_2}{dc_i} + \frac{\partial^2 R_1}{\partial Y_2 \partial Y_2} \frac{dY_2}{dc_j} \frac{dY_2}{dc_i} \\ \frac{\partial^2 R_2}{\partial c_i \partial Y_1} \frac{dY_1}{dc_j} + \frac{\partial^2 R_2}{\partial c_i \partial c_j} + \frac{\partial^2 R_2}{\partial Y_1 \partial c_j} \frac{dY_1}{dc_i} + \frac{\partial^2 R_2}{\partial Y_1 \partial Y_1} \frac{dY_1}{dc_j} \frac{dY_1}{dc_i} \end{bmatrix} \tag{C.28}$$

For each element i, there are M systems of the form shown above, one for each uncertain variable j. Consequently, the system must be solved a total of $M^2 = 81$ times, corresponding to all combinations of (i, j). However, since the second total derivative matrix, or Hessian, is symmetric, only 45 distinct entries need to be computed. This applies because Clairaut's theorem ([17]) is satisfied: the second derivatives of the coupled functions are continuous.

Similarly to the residual function's second-order derivatives, the objective function's ones are:

$$\frac{d^2 \vec{f}}{dc_i dc_j} = \frac{\partial^2 \vec{f}}{\partial c_i \partial c_j} + \frac{\partial^2 \vec{f}}{\partial c_i \partial \vec{Y}} \frac{d\vec{Y}}{dc_j} + \left(\frac{\partial^2 \vec{f}}{\partial \vec{Y} \partial c_j} + \frac{\partial^2 \vec{f}}{\partial^2 \vec{Y}} \frac{d\vec{Y}}{dc_j} \right) \frac{d\vec{Y}}{dc_i} + \frac{\partial \vec{f}}{\partial \vec{Y}} \frac{d^2 \vec{Y}}{dc_i dc_j} \tag{C.29}$$

C.2.1 Constructing the Second-Order Partial Derivatives

The general expression for the second-order derivatives has been established. The corresponding systems are populated using values extracted from the FS equation system, in a procedure that directly follows from the equations formulated for the first-order derivative systems. The coupled functions' derivatives, as were presented in Eq. C.16, are differentiated once more to obtain the second-order derivatives:

$$\begin{aligned}
\frac{d^2 I_x}{dc_i dc_j} &= \frac{dP_{ACS}}{dc_i}\frac{dprt1}{dc_j} + prt1\frac{d^2 P_{ACS}}{dc_i dc_j} + \frac{dprt2}{dc_j} \\
\frac{d^2 P_{ACS}}{dc_i dc_j} &= \frac{dI_x}{dc_i}\frac{dprt3}{dc_j} + prt3\frac{d^2 I_x}{dc_i dc_j} + \frac{dprt4}{dc_j}
\end{aligned} \tag{C.30}$$

Thus, the new system is:

$$\begin{bmatrix} 1 & -prt1 \\ -prt3 & 1 \end{bmatrix} \begin{bmatrix} \frac{d^2 I_x}{dc_i dc_j} \\ \frac{d^2 P_{ACS}}{dc_i dc_j} \end{bmatrix} = \begin{bmatrix} \frac{dP_{ACS}}{dc_i}\frac{dprt1}{dc_j} & +\frac{dprt2}{dc_j} \\ \frac{dI_x}{dc_i}\frac{dprt3}{dc_j} & +\frac{dprt4}{dc_j} \end{bmatrix} \tag{C.31}$$

It is clear that the matrix on the left-hand side is the exact same one as with the first order derivative analysis, which has been explained to be the $\frac{\partial \vec{R}}{\partial \vec{Y}}$. That means that no additional matrix inversion will be necessary. The terms, or functions, $prt\_i, \quad i = 1, 2, 3, 4$ must be differentiated with respect to the uncertainty c_j, for the expression to be completed:

$$\begin{aligned}
\frac{d\,prt1}{dc_j} &= \frac{\partial prt1}{\partial P_{ACS}} \cdot \frac{dP_{ACS}}{dc_j} + \frac{\partial prt1}{\partial c_j} &&= \frac{\partial I_{x_i}^2}{\partial P_{ACS} \partial P_{ACS}} \cdot \frac{dP_{ACS}}{dc_j} + \frac{\partial I_{x_i}^2}{\partial P_{ACS} \partial c_j} \\
\frac{d\,prt2}{dc_j} &= \frac{\partial prt2}{\partial P_{ACS}} \cdot \frac{dP_{ACS}}{dc_j} + \frac{\partial prt2}{\partial c_j} &&= \frac{\partial I_{x_i}^2}{\partial c_i \partial P_{ACS}} \cdot \frac{dP_{ACS}}{dc_j} + \frac{\partial I_{x_i}^2}{\partial c_i \partial c_j} \\
\frac{d\,prt3}{dc_j} &= \frac{\partial prt3}{\partial I_x} \cdot \frac{dI_x}{dc_j} + \frac{\partial prt3}{\partial c_j} &&= \frac{\partial P_{ACS}^2}{\partial I_x \partial I_x} \cdot \frac{dI_x}{dc_j} + \frac{\partial P_{ACS}^2}{\partial I_x \partial c_j} \\
\frac{d\,prt4}{dc_j} &= \frac{\partial prt4}{\partial I_x} \cdot \frac{dI_x}{dc_j} + \frac{\partial prt4}{\partial c_j} &&= \frac{\partial P_{ACS}^2}{\partial c_i \partial I_x} \cdot \frac{dI_x}{dc_j} + \frac{\partial P_{ACS}^2}{\partial c_i \partial c_j}
\end{aligned} \tag{C.32}$$

Substituting the derivatives of Eqs. C.32 to the system of Eq. C.31, the system of Eq. C.28 is finally obtained. At this stage, the procedure for extracting partial derivatives required for the computation of second-order total derivatives has been presented, enabling the corresponding systems to be filled with the appropriate values. The AM approach can then be compared with the DD method in terms of computational cost.

C.2.2 Adjoint method

Eq. C.25 shows that there are multiple appearances of the derivatives of the coupled functions $\frac{d\vec{Y}}{d\vec{c}}$ in the formula of the residual function. The first-order total derivatives must be computed through DD and that statement is backed with a simple example: the first instance of the derivatives in Eq. C.25 is in the term:

$$\frac{\partial^2 \vec{R}}{\partial \vec{c} \partial \vec{Y}} \frac{d\vec{Y}}{d\vec{c}}$$

The first matrix is multiplied with the coupled derivatives matrix, of size $3 \times M = 3 \times 9$. Supposing the first-order derivatives of the objective function were obtained through the AM, the coupled functions' derivative has not been computed-and stored. That means that for the computation of this term (and many others of similar form) the coupled functions' derivatives must be substituted (as per Eq.C.6) as was done in the AM of the previous chapter. The term thus would become:

$$\frac{\partial^2 \vec{R}}{\partial \vec{c} \partial \vec{Y}} \left(\frac{\partial \vec{R}}{\partial \vec{Y}} \right)^{-1} \frac{\partial \vec{R}}{\partial \vec{c}}$$

Now the first matrix must be multiplied with a $N_Y \times N_Y$ matrix and then with a $N_Y \times M = 3 \times 9$. Because of the increased complexity of the terms of eq. C.25 coupled with the number of times the coupled functions' derivative is used, the substitution of the first derivatives just increases the cost of the problem. Generally put, every high-order derivative takes advantage of the AM only for the highest-order derivative, while every other before it must be computed using DD.

The direct method for the second derivatives solves, for every element i, Eq. C.28, M systems of size $N_Y \times N$. Immediately afterwards Eq. C.29 is solved, demanding the computation of the system $\frac{\partial \vec{f}}{\partial \vec{Y}} \frac{d^2 Y_2}{dc_i dc_j}$, which is the multiplication of a $M \times N_Y$ matrix with the $\frac{d^2 Y_2}{dc_i dc_j}$, of size $N_Y \times M$. The adjoint method for the second derivatives offers the alternative, as was done with the adjoint for the first-order derivatives. Now, the system to be solved is:

$$\frac{d^2 \vec{f}}{dc_i dc_j} = \frac{\partial^2 \vec{f}}{\partial c_i \partial c_j} + \frac{\partial^2 \vec{f}}{\partial c_i \partial \vec{Y}} \frac{d\vec{Y}}{dc_j} + \left(\frac{\partial^2 \vec{f}}{\partial \vec{Y} \partial c_j} + \frac{\partial^2 \vec{f}}{\partial^2 \vec{Y}} \frac{d\vec{Y}}{dc_j} \right) \frac{d\vec{Y}}{dc_i} - \underbrace{\frac{\partial \vec{f}}{\partial \vec{Y}} \left(\frac{\partial \vec{R}}{\partial \vec{Y}} \right)^{-1}}_{\Psi^T} \cdot \boldsymbol{B} \quad \text{(C.33)}$$

The adjoint matrix $[\Psi]$ is the exact same one as its previous presentation on the first derivatives. Again, per element i, the adjoint system scales with N_f, not M. Overall every system presented above must be reiterated, for the rest i elements.

Cost Comparison

The computational costs of the methods $DD - DD$ and $DD - AM$ are finally compared.

Direct method — computational cost

First row ($i = 0$)

- **Step 1:** Evaluation of
$$\left(\frac{\partial \vec{R}}{\partial \vec{Y}}\right)^{-1} \mathbf{B}.$$
  Each element of the resulting $(N_Y \times M)$ matrix requires N_Y terms. The total cost is therefore
$$MN_Y^2 \text{ terms.}$$
- **Step 2:** Evaluation of
$$\frac{\partial \vec{f}}{\partial \vec{Y}} \cdot \frac{d^2\vec{Y}}{dc_i\, dc_j},$$
  corresponding to a matrix multiplication of size $(N_f \times N_Y) \cdot (N_Y \times M)$. Each element of the resulting $(N_f \times M)$ matrix requires N_Y products, giving a total of
$$MN_YN_f \text{ terms.}$$

The total cost for the first row is, then,

$$MN_Y^2 + MN_YN_f = MN_Y(N_Y + N_f).$$

Second row ($i = 1$)

- **Step 1:** Construction of a $(N_Y \times (M - 1))$ matrix, requiring
$$(M - 1)N_Y^2 \text{ terms.}$$
- **Step 2:** Matrix multiplication producing a $(N_f \times (M - 1))$ matrix, requiring
$$(M - 1)N_YN_f \text{ terms.}$$

The total cost for the second row is:

$$(M-1)N_Y^2 + (M-1)N_Y N_f = (M-1)N_Y(N_Y + N_f).$$

General case (i-th row)

For the i-th row, the number of remaining columns is $M - i$. The corresponding computational cost is:

$$(M-i)N_Y^2 + (M-i)N_Y N_f = (M-i)N_Y(N_Y + N_f).$$

Total cost of the direct method

Summing over all rows,

$$\sum_{i=0}^{M-1}(M-i)N_Y(N_Y+N_f) = N_Y(N_Y+N_f)\left(M + (M-1) + \cdots + 1\right).$$

Using the identity

$$\sum_{k=1}^{M} k = \frac{M(M+1)}{2},$$

the total computational cost is:

$$\boxed{\frac{M(M+1)}{2} N_Y(N_Y+N_f)}$$

The final product, for $M = 9$, amounts to $45N_Y(N_Y + N_f)$. That gives 450 *cost units* (*cus*) for $N_Y = 2$, and 810 *cus* for $N_Y = 3$.

Adjoint method — computational cost

First row ($i = 0$)

- **Step 1:** Evaluation of

$$\frac{\partial \vec{f}}{\partial \vec{Y}}\left(\frac{\partial \vec{R}}{\partial \vec{Y}}\right)^{-1}.$$

  Each element of the resulting $(N_f \times N_Y)$ matrix requires N_Y terms. The total computational cost is therefore:

$$N_f N_Y^2 \text{ terms.}$$

- **Step 2:** Evaluation of
$$\Psi^T \cdot \mathbf{B},$$
corresponding to a matrix multiplication of size $(N_f \times N_Y) \cdot (N_Y \times M)$. Each element of the resulting $(N_f \times M)$ matrix requires N_Y products, yielding a total of
$$M N_Y N_f \text{ terms.}$$

The total cost for the first row is:

$$N_f N_Y^2 + M N_f N_Y = N_f N_Y (N_Y + M).$$

General case (i-th row)

Following the same reasoning, for the i-th row the number of remaining columns is $M - i$. The corresponding computational cost is:

$$N_f N_Y \big(N_Y + (M - i)\big).$$

Total cost of the adjoint method

Summing over all rows,

$$\sum_{i=0}^{M-1} N_f N_Y \big(N_Y + (M - i)\big) = N_f N_Y \left(M N_Y + \sum_{k=1}^{M} k \right)$$

Similarly, the total computational cost becomes:

$$\boxed{N_f N_Y \left(N_Y + \frac{M(M+1)}{2} \right)}$$

The final product, for $M = 9$, amounts to $N_f N_Y \, (N_Y + 45)$. This time, a system with $N_Y = 2$ costs 282 cus, while a system with $N_Y = 3$ costs 432 cus. Table C.8 is drawn to compare the two methods:

Size of Operations	
$DD-DD$	$\frac{M(M+1)}{2}N_Y(N_Y+N_f)$
$DD-AM$	$N_fN_Y(N_Y+\frac{M(M+1)}{2})$

Table C.8: Direct vs Adjoint method

Again, if the case had $N_Y \to \infty$, the direct to adjoint cost ratio $\frac{DD_{cost}}{AM_{cost}} \to \frac{M^2}{N_f}$ when the Hessian is not symmetric and $\frac{DD_{cost}}{AM_{cost}} \to \frac{M(M+1)}{2N_f}$ when it is. The resulting values of the $DD-DD$ and $DD-AM$ are identical, similarly to the previous chapter. The accuracy of the computed derivatives this time is not proven using the respective FD results: instead, the accuracy is proven by the results of the UQ presented in Chapter 4.

Derivative Computation Cost Relative to the Primal System

The $DD-DD$ method requires the solution of $\frac{M(M+1)}{2} = 45$ systems, each of size $N_Y \times N_Y$. To provide a reference, the $DD-DD$ cost is then:

$$\boxed{(DD-DD)_{cost} \approx 45 \ \ primal_{cost}}$$

Consequently, the $DD-AM$ cost for this case specifically, is:

$$\boxed{(DD-AM)_{cost} \approx 45 \ \frac{AM_{cost}}{DD_{cost}} \ \ primal_{cost} \approx 24 \ \ primal_{cost}}$$

That concludes the overall costs of the entire MoM procedure:

For $DD-DD$:

$$\boxed{MoM_{(DD-DD)} = \underbrace{9 \ \ primal_{cost}}_{DD} + \underbrace{45 \ \ primal_{cost}}_{DD-DD} = 54 \ \ primal_{cost}}$$

For $DD-AM$:

$$\boxed{MoM_{(DD-AM)} = \underbrace{9 \ \ primal_{cost}}_{DD} + \underbrace{24 \ \ primal_{cost}}_{DD-AM} = 33 \ \ primal_{cost}} \tag{C.34}$$

In conclusion, the computation of derivatives in a MD system follows the same fundamental principles as in a single-discipline case. The residual equations, which define the converged state of the system, serve as the governing relations for the system variables. In this context, the coupled functions assume the role of state variables, and the differentiation process retains the structure and interpretation of standard sensitivity analysis. Once convergence is achieved under the MDF formulation, the residual system is formed, with one equation per coupled function, and the derivatives are obtained accordingly.

The FS system is relatively simple, as it does not involve spatially distributed fields such as velocity or pressure. All quantities are scalar, and the problem dimension is determined solely by the number of coupled functions—two or three, depending on the torque scenario (C.10). This reduced dimensionality simplifies the formulation and enables a fully analytical treatment of the derivatives.

Bibliography

[1] OpenTURNS Contributors. *OpenTURNS: Open source initiative for the Treatment of Uncertainties, Risks'N Statistics*. `https://openturns.github.io/openturns/latest/usecases/use_case_fire_satellite.html`. OpenTURNS version 1.26 documentation.

[2] James R. Wertz and Wiley J. Larson. *Space Mission Analysis and Design*. Torrance, CA: Microcosm Press, 1999.

[3] Shankar Sankararaman and Sankaran Mahadevan. "Likelihood-based approach to multidisciplinary analysis under uncertainty." In: *Journal of Mechanical Design* 134.3 (2012), p. 031008.

[4] Khaled Zaman. "Modeling and management of epistemic uncertainty for multidisciplinary system analysis and design." PhD thesis. USA: Vanderbilt University, 2012.

[5] Thomas Bäck. *Evolutionary Algorithms in Theory and Practice*. Oxford University Press, 1996.

[6] Joaquim R. R. A. Martins, Peter Sturdza, and Juan J. Alonso. "The Complex-Step Derivative Approximation." In: *ACM Transactions on Mathematical Software* 29.3 (2003), pp. 245–262.

[7] Jorge Nocedal and Stephen J. Wright. *Numerical Optimization*. 2nd. Springer, 2006.

[8] Reuven Y. Rubinstein and Dirk P. Kroese. *Simulation and the Monte Carlo Method*. 3rd. Wiley, 2016.

[9] Dongbin Xiu. *Numerical Methods for Stochastic Computations: A Spectral Method Approach*. Princeton: Princeton University Press, 2010.

[10] Evangelos Papoutsis-Kiachagias. "Adjoint Methods for Robust Aerodynamic Shape Design with Third-Derivative Computation: Application to One-Dimensional Ducts." MA thesis. Athens, Greece: National Technical University of Athens, Laboratory of Thermal Turbomachines, 2009.

[11] Isaac Newton. *Philosophiæ Naturalis Principia Mathematica*. Latin. London: Royal Society, 1687.

[12] Jaroslaw Sobieszczanski-Sobieski, Joachim S. Agte, and Ronald R. Sandusky. *Bi-Level Integrated System Synthesis (BLISS)*. Tech. rep. TM-1999-209758. NASA, 2000.

[13] Natalia M. Alexandrov and Robert M. Lewis. *Analytical and Computational Aspects of Collaborative Optimization*. Tech. rep. TM-2002-211804. NASA, 2002.

[14] Joaquim R. R. A. Martins and Andrew B. Lambe. “Multidisciplinary Design Optimization: A Survey of Architectures.” In: *AIAA Journal* 51.9 (2013), pp. 2049–2075.

[15] M. D. McKay, R. J. Beckman, and W. J. Conover. “A Comparison of Three Methods for Selecting Values of Input Variables in the Analysis of Output from a Computer Code.” In: *Technometrics* 21.2 (1979), pp. 239–245.

[16] Duncan Cramer. *Fundamental Statistics for Social Research: Step-by-Step Calculations and Computer Techniques Using SPSS for Windows*. London, United Kingdom: Routledge, 1997.

[17] Jerrold E. Marsden and Anthony J. Tromba. *Vector Calculus*. 6th ed. W. H. Freeman, 2012.